The response to referee 1 can be found on the following pages.

Dear reviewer,

thank you for reading the paper and thank you for your feedback. You can find responses to your comments and questions below in blue.

Comments

Overall remarks

It is a well-written paper with enough material to form a substantial contribution to the pitch bearing literature, particularly as there is a dearth of papers about three row roller bearings. As it is a methodology paper, it should be relatively easy to follow the procedure adopted which it is. The flow of the methodology has been clearly illuminated by the well-separated chapters. The reasoning for the methodology has been illuminated properly with enough validation done for each aspect of the method. There are some minor issues which need to be corrected highlighted in the next section. Since the authors validated this method with its relevant assumptions for a specific wind turbine, it may also be good to describe or postulate if this method will work in general for wind turbines with three row roller bearings as well (as much as possible within the limits of confidentiality).

Thank you for the kind words. We believe the method shown is also applicable for other wind turbines that use three-row roller bearings as pitch bearings. Most of the assumptions we took should also hold true for other wind turbines. This information was added to the conclusions.

Specific comments

1. Line 7: The modification of the bearing is mentioned but never discussed further (except in the conclusion). Please either include a line or so in the main text about this. Even if it is confidential, possibly mention this.

   The modification that was undertaken is confidential, this information was added to the introduction.

2. Line 81: The choice of 21 slices for the FEM model is not explained. Why was this value chosen? Is it standard within the extension?

   It was the maximum possible value of springs in the extension at the time we wrote the paper, this information was added to the manuscript. (Side note: Further analyses undertaken by us later show that the amount of laminae used in FE has little impact on the results of the Reusner submodel; this will be published in a separate paper in the future)

3. Line 83: “contacting roller and raceway” may be a better formulation.

   Changed as suggested.

4. Line 88: Unless confidential, possibly mention if the split happens in the inner or outer ring and approximate location. I see a split in Figure 1; this could be highlighted there, too.

   The location of the split is unfortunately confidential. Figure 1 may or may not be representative of the bearing we calculated. This information was added and the split in Figure 1 is now referred to for readers unfamiliar with the concept.

5. Line 198: The reference "Stammler et al.": Please date these references as there are multiple from the same author.

   The date was added (it is from 2024, specifically this sentence is citing the new NREL DG03)

6. Line 316-318: It is mentioned that the Reusner algorithm gives a more accurate load distribution than the FE simulation. It is mentioned later on about it being due to the Hertzian nature of contact algorithm ("For these 72 simulations, the contact pressures of all rollers were determined using a non-Hertzian contact algorithm based on Reusner (1977). Unlike the Hertzian rolling elements used in FE, the non-Hertzian algorithm allows for detection of edge stresses and is more accurate in general."). To make it clearer, the hertzian nature of the FEM model can be explained before this part of the text.

   The sentences "Pressures of these laminae can be calculated using Hertzian theory. However, Hertzian theory simplifies the roller-race contact and may underestimate the real pressure" were added prior to the cited sentences. Furthermore, the wording "This returns a more accurate load distribution" was changed to "This returns a more accurate pressure distribution" to clarify that pressure is the variable of interest here. (This is because, strictly speaking, the load-deflection relationship used in FEM based on ISO 16281 is based on Palmgren, and only the corresponding pressure calculation is based on so-called Hertzian theory).

7. Line 517: About the bending moment and resulting structural deformation playing a larger role in the loading of the radial row than the radial load itself: How exactly does structural deformation happen in this case? What is a possible reason for this? Can there be numbers put to this (if possible)?

   Structural deformation causes the rings of the bearing to deform in ways that are unfortunately difficult to predict without detailed FE simulations (refer to Fig. 4, 5, and 6). In this case, the two contacting points of the radial rollers (the raceway on the"nose" of one ring and the raceway surface on the other) deflect, too, as a result of the global load, in particular the bending moment as it is the highest load acting on the bearing. This deflection of the "nose" and the other contact point of the radial row (evidently) affects the strange, unpredictable load distribution on the radial row more so than the radial force.

   Putting numbers to this is unfortunately very difficult. In this paper, we are attempting that with these sentences:

   The radial load Fr is very small compared to the load rating Cr of the radial row. Following the above described procedure, the life of the radial row is over 200 times as large as that of the axial row. This is incorrect: the actual life of the radial row is only about 10-15 times as high as that of the axial rows, see Fig. 18.

We are currently not aware of a better way to put numbers to this. The above relative difference may very well differ for other bearings on other turbines, too.

8. Line 527: By a simplified approach like in Eq. 21, do you mean to say that only the axial load (ignoring the Fr mentioned in Eq.21) is to be considered here? Also, it could also be clarified then that since it is a roller bearing, the 10/3 exponent is to be used. Also, for the sake of clarity, is Ca of a single axial row to be used for life?

   No, the load Fr mentioned in Eq. 21 should also be included. We call this approach simplified because it is much simpler than the above described procedure that uses FE simulations, Reusner submodeling, etc.

   We clarified that 10/3 should be used, thank you for the note.

   For a three-row roller bearing, Ca of the entire bearing is always the Ca of a single axial row. This is because the bearing is a so-called double-direction bearing, where an *axial* load only loads one of the rows at a time but never both at once. For bending moments, both rows are loaded at once; but as the definition of Ca refers to an axial load, only one row's Ca is used as the Ca for the entire bearing. This definition follows ISO 281: Refer to ISO 281:2007, Sec. 8.1.1: *The basic dynamic axial load rating for single-row, single-direction or double-direction thrust roller bearing is given by Ca = [...]*

The response to referee 2 can be found on the following pages.

Dear reviewer,

thank you for reading the paper and thank you for your feedback. You can find responses to your comments and questions below in blue.

General remarks:

Well explained and clear structured paper.

Thank you for the kind words.

The graphics are too small and difficult to read.

Most of the graphics use a similar font size to the manuscript text, for images that are difficult to read, the graphics are all high-quality images and zooming in is possible. As there is a lot of information contained in the images we had to make do with the available space, unfortunately.

Some sources only given with name, no further information (year etc.) à e.g. “see Stammler et. al.”

Corrected where we found this issue (also for Keller, Jonathan and Guo, Yi)

Will the use of a full 3D model of the bearing and the time series allow to predict the circumferential location of the rolling contact fatigue failure?

While this was not the focus of this paper, other works by the authors (see https://doi.org/10.1115/1.4055916) can be used to find the area of highest damage likelihood. Of course, with fatigue being a statistical phenomenon, an exact location can never be foreseen.

Data Quality "Fair" due to the confidentiality requirement.

In detail:

Line 7: In comparison to ball bearings, the calculation of roller bearings [..] leading to significantly more degrees of freedom.

A Ball bearings also have many degrees of freedom, if modelled with balls having realistic kinematic behaviour (instead of springs and fixed contact angle) since the contact angle ball to raceway can differ from ball to ball and is strongly load dependent.

This is true for FE modeling, but this sentence was specifically meant to refer to the DOFs in the fatigue calculation. Changed the “[...] the calculation of roller bearings [...]” to “[...] the rolling contact fatigue calculation of roller bearings [...]” to highlight this point.

Line 8: For this paper, the bearing is modified slightly: What does modified slightly mean? Please describe more detailed, if possible.

Unfortunately the details of the modification are confidential. The information that the details are confidential was added to the manuscript.

Line 56-58: Does the roller profile used for the calculation differ between the "confidential" turbine pitch bearing and the more "generale" bearing? If so, how is the influence onto the "normalized" results?

This information is unfortunately confidential.

Line 65: But is it possible to get the ISO life calculations **quantitively** reliable?

In the scope of this paper that's a question we won't answer (yet), but generally we believe so. Look out for future publications from us on this topic.

Line 81-83: Can you explain why 21 springs are used in the FE model, whereas ISO/TS16281 requires min. 30 slices in their roller slice model?

At the time of writing the paper the extension only allowed a maximum of 21 slices, which is why this value was chosen. We included this information in the manuscript. To ensure that this does not falsify the results, we undertook analyses (including custom-built FE models with 31 slices) which showed that the amount of slices in the FE model has little influence on the Reusner submodel so long as the Reusner submodel has sufficient slices; this will be published in a separate paper in the future.

Note also that the Reusner submodel, the results of which are used for the life calculation, did include 30 slices.

Line 88: [..] This split of the ring is considered in the model and the surfaces are connected to each other by an internal frictional contact. [..] Axial clamping force? Bolt preload? Influence bolt preload on roller preload?

The axial clamping force is driven by the bolt preload of the bolts. Each bolt along the circumference is preloaded with the same load which corresponds to the target mounting bolt preload. The higher the bolt preload the higher the preload of the axial rollers on both rows of the bearing.

Line 166-167: Influence of pitch angle might only become more important if the blade model differs circumferentially from its mechanical properties. How is the blade root stiffness modelled, uniform or non-uniform, anisotropic?

The orthotropic material behavior of the blade root / blade dummy composite material is considered in the model. The material model contains direction dependent Young's moduli, Poisson's ratios and shear moduli. For the blade root a blade dummy is used as written in a manuscript, however, further details on this subject are confidential.

Line 220: again the question about blade root model and physical properties around circumference - uniform or non-uniform

As explained above, for the blade root a blade dummy was used. Further details on this subject can unfortunately not be shared.

Line 296-298: Is there a difference for small back and forward motion compared to full rotations in calculating dynamic equivalent load and bearing lifetime? If so, further explanation would help. Have time steps with negligible rotation been ignored, if so what is the minimum pitch angle to be considered?

Time steps with negligible rotation have not been ignored, as there is no clear limit for what constitutes a “negligible” rotation known to us.

Yes, generally, there is a difference for small back and forward motion compared to full rotations in calculating dynamic equivalent load and bearing lifetime. When a bearing is fully rotating, the rotating ring is continuously rotating through the highest loaded zone. All spots on the circumference of the rotating ring thus go through the load zone. When it is oscillating back and forth, only one area on the circumference will be in the highest loaded zone. This is discussed in detail in Menck and Stammler (2024) and we added the following sentence to the manuscript to point this out:

These small oscillations cause the oscillating ring to be almost stationary w.r.t. the load, differing from a rotating bearing, where the rotating ring rotates relative to the load.

Line 310: why 21 laminae in FE compared to min. 30 as per ISO 16281

As explained above, this is in part due to limitations in the extension at the time of writing this paper, however, we ensured that it does not affect the results, details on which will be published in the future. The Reusner submodel does fulfill the minimum requirement of 30 slices.

Figure 14: Graphics of convergence analysis in not convincing compared to line 349. The graphics do not show why 30 lamina is a suitable choice.

They show that for 30 laminae, L10r is within a +-3% range of the reference result using 150 slices. This was the intention of the figure.

Line 405: What is the expected difference in rating life between analysis done on time steps compared to load bins?

This is impossible to answer generally as it highly depends on the binning process. In WES - Review of rolling contact fatigue life calculation for oscillating bearings and application-dependent recommendations for use, Figure 8, we are doing a comparison, but we would assume that for other choices of bins the result can be quite different.

Line 516: What impact will the radial row, at 10-15 times the life of the axial raceways, have on the combined rating life?

A very small impact. As you can see in Fig. 20, Column “Radial”, even though the radial row approximations are sometimes wildly off the reference (“FE to Reusner”), the combined life in the “Whole bearing” column deviates very little.

Line 519-520: Will radial load be added to eq. ax. load Pa and compared with axial load capacity Ca? Further explanation required for formula.

Yes, that’s the way Eq. 21 is generally employed. Added the sentence “The radial load is thus included in the dynamic axial load” after Eq. 21 to clarify this point.

Line 529: Further explanation required, also in relation to formula above. Normally ball bearings have higher k factor on moments compared to axial rows of 3 row roller bearings if calculating axial and radial raceways separately on 3 row roller bearings.

We are unsure which k factor you are referring to here, as this calculation is the first we are aware of for a three-row roller bearing in the published literature.

Line 566: What would be a high edge stress?

A significant increase of the stresses at the roller edges as compared to the roller center. We are unaware of any strict definitions (e.g., 50% higher than the roller center… or similar), but the phenomenon of high edge stresses is generally recognized in the literature, see ISO 16281, Harris and Kotzalas (2007), etc.

Line 581: What is the expected failure mode of a three-row roller bearing

We believe this question is beyond the scope of this paper, but rolling contact fatigue is one possible failure mechanism among a number of possible failure mechanisms.

The response to community comment 1 can be found on the following pages.

Dear reviewer,

thank you for reading the paper and thank you for your feedback. You can find responses to your comments and questions below in blue.

In this paper, the authors describe a methodology for a rolling contact rolling contact fatigue life calculation for a three-row roller bearing. An example calculation is provided. Several interesting clarifications compared to the approach described in the NREL DG03 are made, along with some interesting technical results gleaned from the example calculations . I was going to read this paper in depth no matter what, and in doing so, figured I would make some hopefully helpful clarifying comments.

Thank you for the kind words and for your efforts.

Abstract

- Line 8: I'm not sure I understand "the bearing is modified slightly" pertains to the model or the actual bearing (or both). I believe this really relates to the aspect of confidentiality in the next sentence. To be honest, I think stating "Exemplary calculations…" states all that is needed here, as the actual dimensions or other structural and material aspects of the bearing are not given in the paper. Another option might be stating "Exemplary calculations are carried out using a slightly modified version of an extensively validated FE model of a three-row roller bearing of a wind turbine."
  The modification pertains to the bearing model used for this paper only.
  The sentence was changed as suggested.
- Lines 9-10: I understand this sentence "Since…confidentiality…", but I'll admit it feels a bit odd to state in the Abstract. I recommend it be deleted here and only stated in the text if really necessary. Indeed, this is done on line 56 and it feels sufficient and appropriate there.
  Removed the note about confidentiality from the abstract as suggested.
- In the Abstract, I do recommend adding a statement better summarizing the main findings in the paper. From the Conclusions my main takeaway was that "The axial rows were found to have a much lower fatigue life than the radial row, and thus the axial rows are the main determinant of the fatigue life of the bearing. They also were shown to have a much lower uncertainty than the radial row."
  Added the sentence as suggested.

1 Introduction

- Lines 21-22: Strictly speaking, cyclic changes in subsurface stress don't *cause* inclusions or material defects themselves to grow, so I think slightly modifying this sentence to something like

  "Cyclic changes in sub surface stress near inclusions or material defects cause microcracks that grow into larger, macroscopic spalls."

  Changed as suggested

2.1 FE bearing model and validation

- Lines 106-108: I'm not sure I understand the meaning of "The scatter bars in the plots indicate the fluctuation in the measured signals which is caused by the pitch movements of the bearing". As is, I took this to mean that the uncertainty would be in the horizontal axis rather than the vertical. Rather, I interpret this statement to mean that the rolling elements may not be in exactly the same location relative to the strain gauge as the bearing rotates (pitches) and the rollers orbit – I would assume this to possibly be related to some amount of sliding, even very small. Is that correct? So maybe "…caused by small differences in the locations of the rollers relative to the strain gauge as the bearing pitches" is a clearer way to say it? I can understand then that for smaller bearings this effect is more pronounced (as the size of the gauge is a larger proportion to the bearing circumference). I also think adding "…differently pronounced between both test bearings in Figure 6" would be helpful in line 108.
  The strain gauges are in one constant position but as the bearing rotates, they fluctuate somewhat. We have observed this behavior on all our test rigs and it is not specific to the one in this paper, neither can we say for sure that it is due to the rolling elements' movement, as previous publications have shown that manufacturing anomalies within the tolerances can also affect the strain gauge results (https://doi.org/10.1016/j.finel.2024.104268). Differences in the scatter bars are observable in Figs 4-6, not only 6.

3.1.1 Approximation of Fx and Fy for blade 1

- I think Section 3.1.1 is quite interesting as it's the first time I have seen anyone look at and propose this. However, I wonder, if one is doing the aeroelastic simulations anyway, what is the value of approximating Fx and Fy? Can the authors comment? Is this maybe because if one is interested in relating field testing measurements of blade root loads to RCF calculations, it is only really possible to measure the blade root moment and not the force? If this is the intent, it might be worthwhile mentioning it.
  The intent here is just to be able to reduce the number of simulations that are being done in FE. It is only feasible to do a small number of FE simulations and therefore we need to reduce the DOFs as much as possible. This approximation of Fx and Fy is thus used to perform FE simulations that only use Mres, the load angle, and Fz as DOFs, but still include a "realistic" Fx and Fy by determining them based on the bending moment Mres and its load angle.

3.1.2 Choice of grid simulation points for Fz for blade 1

- Line 212: A very minor point that the statement "Since high forces are those that affect the life the most" is really only partially true – it's really the combination of force and the

number of cycles at that force that affect life the most. At least the rolling contact fatigue life. Or maybe the authors intend this statement to be generally the "life" due to all failure modes, rather than just the rolling contact fatigue life.
You are entirely correct in stating that high forces in combination with movement affect the life, but here we are discussing one given load distribution and we are commenting on the loads within that load distribution. In that context, it is not possible for the area around 180° to have significantly less movement than that around 90° unless (very) strange slippage effects occur.
Changed the sentence to "*Since highly loaded rolling elements are those that affect the life the most, this result is adequate for the life calculation*" to clarify this.

3.3 Loads at blades 2 and 3

- Line 240: Can a citation for "Note this influence of blade 2 and 3 is more significant for other damage modes such as ring cracks" be added?
  There is no clear source for this but " Multi-MW Blade Bearing Applications –Advanced Blade Bearing Design Process and Pitch Bearing Modul Development Trends" by Daniel Becker, presented at IQPC 2023, states
  Edgewise loads do not play a significant role for raceway fatigue, but do for ring / bolt fatigue …
  Edgewise loads are influenced by blades 2 and 3, hence their effect on ring cracks.
  However as no clearer source could be provided we changed the sentence to
  Note this influence of blade 2 and 3 is likely more significant for other damage modes such as ring cracks, as they influence the edgewise loads, which are known to affect ring cracks (Becker, 2023)

4 Rolling contact fatigue life for individual load cases

- Line 256: The NREL DG03 describes more than 1 method to calculate rolling contact fatigue life, so I recommend this sentence be revised to "The rolling contact fatigue life calculation adheres closely to the ISO/TS 16281-based methodology described in the NREL DG03 (Stammler et al. 2024)."

  Changed as suggested

- Line 263: I'm not sure if the adjective "operational" for fatigue life is really needed, compared to the other uses in the document of simply "fatigue life" or "rolling contact fatigue life". If "operational" does not have an intended meaning, I recommend deleting it.
  Deleted as suggested.

5.2 Combined operating life

- Line 493: What is the variable x_i?
  It's a multiplier (based on the Weibull distribution), this is stated 5 lines before (*This process takes into account the multipliers x_i. […])*

- Line 501: I am often struck of our practice of doing quite detailed load and pressure calculations, but then when calculating a modified fatigue life, we use relatively large modification factors that are "based on experience". In the case of pitch bearings, the NREL DG03 suggests a_srv = 3. Having said that, outside of a relatively small community I'm not sure how many end users are aware of such estimates when compared to the basic fatigue life calculations themselves. With that opinion in mind (and a bit of humility and honesty), I recommend revising this sentence to at lease allude to this with something like "Further factors may be multiplied with this basic fatigue life yielding a modified fatigue life. The highest is a suggested value of 3 based on experience of the manufacturer, as well as on……..(Stammler et al. 2024)."
  Changed to:
  Further factors may be multiplied with this basic fatigue life yielding a modified fatigue life. These values may be based on experience of the manufacturer, as well as on properties of the bearing like its hardening depth, raceway hardness, or desired reliabilities other than 90 % used for L10, see Stammler et al. (2024). The highest factor is a suggested value of 3, see Stammler et al. (2024)

5.3 Simplified life calculation

- I suggest adding a clarification to the middle of the paragraph from lines 510 to 513 summarizing the NREL DG03 simplified calculation method, based on previous correspondence with the authors. The main reason being that Eq. 13 refers to m = 1 to 3, with the axial rows (m = 1 and 2) and radial row (m = 3). So, a reader is again expecting m = 1 to 3 here. However, my understanding of the authors intent is that only two parts are used: an axial row (m =1) and the radial row (m=3). That is, the difference is that only 1 of the axial rows are used, not that the radial and axial rows are calculated separately (they are calculated separately both in section 4.1 and here in section 5.3). Thus, using consistent terminology as section 4.1 and Eq. 13 but highlighting the important difference, I believe it is clearer to state here "They propose calculating the life of only one of the two axial rows L10,2 = (Ca/Pa)^10/3 because it is assumed only one axial row at a time carries the axial load, where Pa = …, and combining it with the life of the radial row L10,3 = (Cr/Pr)^10/3, where Pr = … The life of the entire bearing is then calculated using Eq. 13 from just these two results (i.e. m = 2 to 3)." I believe this is the clearest description.

  No, there appears to be a misunderstanding, both axial rows are used for the calculation of L10,a. The load rating Ca is defined for a single row, since an axial bearing under an *axial* load would only carry on one of the rows. This definition follows ISO 281 (see our reply to RC1, comment 8). For a *bending moment*, both rows carry load, and hence for the *life*, the loads of both rows are considered.

- Line 516: Another minor clarification, difference in radial load life between the methods is valid for the bearing and turbine loads studied in this paper, but I agree it is a trend likely to occur in other cases. With that, I recommend adding "This is incorrect: for the current example, the actual life of the radial row…."
  Changed as suggested
- Line 527: Similar to my previous comment regarding lines 510 to 513, I recommend another clarification here such as "Thus, for an even more simplified approach than the NREL DG03, the life of the bearing L10 = (Ca/Pa)^10/3 can be determined using from just Eq. 4 for Ca and Eq.21 for Pa, if the factor kM is adjusted. This simplified approach can be useful for parametric studies, for example of the effect of different pitch bearings, wind speed distributions, or controllers."

Changed as suggested

6 Equivalent time for an accelerated fatigue life test on a pitch bearing test rig

- In general, this section “sticks out” a bit, as it’s not really connected to the rest of the paper. I wonder if it would be worthwhile to highlight the fact that such a fatigue life test could be useful in assessing uncertainties with the radial row fatigue life, or the factor kM. I understand from the rest of the manuscript that the axial rows have a lower fatigue life….I suppose…but can one really say that confidently with such a high degree of uncertainty on the radial row fatigue life? Can something be added here that better connects this section with the rest of the paper?
  We agree that the section is poorly connected to the rest of the paper and adds little to the available literature. Section 6 and all references to it were therefore removed from the manuscript.

7 Conclusions

- Line 549: Please add “…approach to calculate the fatigue life

of…”

Added as suggested

Minor grammatical comments:

- Line 32 (and elsewhere): ISO/TS 16281 (2008 edition) was recently revised and upgraded from a technical specification to international standard as ISO 16281 (2025 edition). It may be worthwhile considering whether to refer to the well-known TS versus the IS, depending on whether or not there are any relevant differences for this manuscript.
  There are no relevant differences between ISO/TS 16281 and ISO 16281:2025 for this manuscript, therefore, all references were changed to ISO 16281. This does not include any references to the approach in NREL DG03 based on ISO/TS 16281, where the reference to ISO/TS 16281 remains, as here for example in the introduction:
  The calculation approach shown herein follows closely the abovementioned NREL DG03, the rolling contact fatigue calculation approach of which is based closely on ISO/TS 16281 (now replaced by ISO 16281).

  Neither this manuscript nor NREL DG03 are affected by any differences between ISO/TS 16281 and ISO 16281:2025 to the best knowledge of the authors.
- Lines 39 and 45 (and elsewhere): “Keller, Jonathan and Guo, Yi” should read “Keller and Guo, 2022”
  corrected
- Line 47 (and elsewhere): “Stammler et al.” should be “Stammler et al., 2024”.
  corrected

All relevant changes to the manuscript are also visible in the following document with tracked changes.

Rolling contact fatigue calculation of a three-row roller pitch bearing in a wind turbine

Oliver Menck[1], Florian Schleich[1], and Matthias Stammler[1]

[1]Fraunhofer Institute for Wind Energy Systems IWES, 21029 Hamburg, Germany

Correspondence: Oliver Menck (oliver.menck(at)iwes.fraunhofer.de)

Abstract. Rolling contact fatigue calculations of wind turbine pitch bearings have to consider the oscillating operation and the complex, dynamic load distribution in the bearing. The present work proposes a methodology to calculate the life of a pitch bearing that is a roller bearing, specifically a three-row roller bearing. Previous publications in this field have discussed the life calculation of ball pitch bearings. Methodologies applicable to any pitch rolling bearing are partly improved upon in the present work. Several aspects not applicable to roller bearings are re-thought. In comparison to ball bearings, the rolling contact fatigue calculation of roller bearings adds another level of complexity, since they have a long contact which is typically discretized if strong deformation is present, leading to significantly more degrees of freedom. Exemplary calculations are carried out using a slightly modified version of an extensively validated FE model of a three-row roller bearing of a wind turbine. ~~For this paper , the bearing is modified slightly. The results of the life calculation are put in relation to an accelerated fatigue test on a pitch bearing test rig. Since some of the results can nonetheless not be shown for reasons of confidentiality, the focus of this paperis on the methodology used~~This paper focuses on the methodology used to calculate the life. The axial rows were found to have a much lower fatigue life than the radial row, and thus the axial rows are the main determinant of the fatigue life of the bearing. They also were shown to have a much lower uncertainty than the radial row using the approach proposed in this paper.

1 Introduction

Modern wind turbines contain a pitch bearing (also called rotor blade bearing) at the root of each rotor blade which is used to rotate the blade along its longitudinal axis. This is used to start and stop the turbine and to control the loads acting on it (Burton et al., 2011). While pitch bearings in older turbines mostly performed relatively little movement, newer turbines increasingly use control mechanisms that are intended to reduce fatigue loading on various components of the turbine by dynamically adapting the pitch angle during operation (Bossanyi, 2003). This increases movement of the pitch bearing and therefore decreases its rolling contact fatigue (RCF) life.

RCF is a fatigue damage type that is caused by rolling elements in a rolling bearing repeatedly moving over the raceway. Movement of the rolling element, even without any friction, causes changes in sub surface shear stress. This shear stress, particularly the orthogonal shear stress, is thought to be the initiating stress that causes RCF (Lundberg and Palmgren, 1947), though other stresses have been proposed to be the origin of RCF as well (Sadeghi et al., 2009). Cyclic changes in sub surface stress ~~cause~~ near inclusions or material defects ~~to~~ cause microcracks that grow into larger, macroscopic spalls. These can

cause failure of a bearing. Fatigue is a stochastic phenomenon; the life of the bearing until a spall occurs can therefore only be determined for a given probability. Industry-typical is the use of L_{10}, which denotes the life for 90 % reliability, i.e., the operational time until which 90 % of bearings do not have any visible spall damage on their raceways.

Pitch bearings can experience a number of failure mechanisms (Stammler et al., 2020). Some of these are relatively untypical failure modes that specifically affect pitch bearings due to their unusual operational behavior, such as ring fracture, which occurs due to the variation in external bending moment loading (Becker et al., 2022), or wear damages on the raceway, which can be caused by the oscillatory movement patterns of the bearing (Schwack, 2020; Stammler, 2020). Rolling contact fatigue on the other hand is a more common type of damage that can, in principle, affect any bearing in any operational scenario if the loads are sufficiently high and the bearing moves (rotates or oscillates) sufficiently. The calculation methods for rolling contact fatigue are thus standardized in ISO (see ISO 281, ISO/TR 1281-1, ISO/TR 1281-2, ISO ~~/TS~~ 16281), although a number of other approaches also exist in the literature. Nonetheless, for the application in wind turbine pitch bearings, a number of additional questions arise, particularly due to the flexibility of the bearing rings, which necessitate finite element (FE) simulations, and due to the stochastic variation in loads and movement due to the wind.

Although there are a number of pitch bearing types that are used by different manufacturers, the most common type is probably the double-row four-point bearing. Publications on pitch bearings reflect this fact as the vast majority of them cover double-row four-point bearings, see for instance (Schwack et al., 2016b, a; Stammler et al., 2018; Lopez et al., 2019; Menck et al., 2020; Leupold et al., 2021; Menck et al., 2022; Keller and Guo, 2022; Graßmann et al., 2023; Menck, 2023; Rezaei et al., 2023; Escalero et al., 2024; Rezaei et al., 2024; Schleich et al., 2024). Far fewer publications have been written on the subject of roller bearings as pitch bearings, see (Stammler et al., 2018) for a load calculation of a roller pitch bearing and (Stammler, 2023) for a wear test program on roller pitch bearings. While still less common than double-row four-point bearings, anecdotally, roller bearings seem to become more common types of pitch bearings for increasingly larger turbines.

While many of the aforementioned publications on double-row four-point bearings present or apply life calculation approaches (Schwack et al., 2016b; Lopez et al., 2019; Menck et al., 2020; Leupold et al., 2021; Keller and Guo, 2022; Menck, 2023; Rezaei et al., 2023; Escalero et al., 2024), there are almost no publications on the life calculation of roller bearings aside from the NREL DG03 (Stammler et al., 2024), which is a guideline for pitch bearing calculation, and industry presentations that give limited detail on the calculation approach (Becker, 2024). Roller bearing life calculations include an additional degree of complexity compared to ball bearing life calculations, because rollers are profiled in order to prevent edge stresses (Harris and Kotzalas, 2007). Profiles are manufacturer-dependent and their use necessitates numerical contact models, since simple Hertzian equations cannot accurately determine the stresses that occur in a roller-raceway contact; they may only approximate it for ideal contact conditions (Lundberg, 1939).

The given paper aims to show a comprehensive approach for the life calculation in a three-row roller type pitch bearing in a modern wind turbine. A three-row roller bearing contains two axial rows, one for positive axial loads and one for negative ones, and a radial row for radial loads. It is depicted schematically in Fig. 1 with the raceway nomenclature used in this paper. The turbine used for the calculation is multi-MW product. Several information as bearing dimension, roller profile, calculation results cannot be shared for confidentiality reasons. The bearing model used for this paper is also slightly modified in a manner

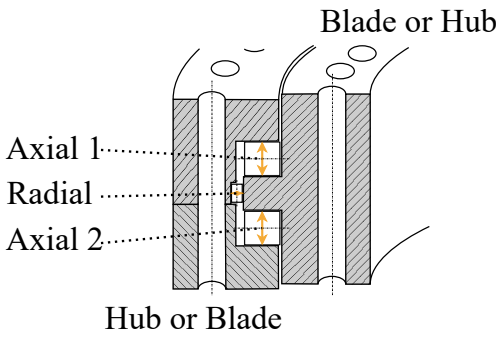

Figure 1. Example three-row roller bearing with raceway nomenclature and hub and blade locations. Hub either attaches to either inner or outer ring, blade attaches to the other ring.

that is confidential. Instead normalized results are shown and roller profiles are defined using ISO profiles according to ISO ~~/TS~~ 16281.

The calculation approach shown herein follows closely the abovementioned NREL DG03, the rolling contact fatigue calculation approach of which is based closely on ISO/TS ~~16281.~~ 16281 (now replaced by ISO 16281). Some previous papers have criticised ISO standards for supposedly being unreliable for large scale pitch bearings, see (Lopez et al., 2019; Potočnik et al., 2010), but no evidence of this has been given in the literature known to the authors. Results from previous life calculations (Schwack et al., 2016b; Menck et al., 2020) of double-row four-point bearings were so absurdly low that they could not possibly be accurate. At the time of writing, the authors assume that this discrepancy can be done away with by modifying smaller aspects of the presented life calculation method, like for instance by applying different life modification factors. There is no evidence known to the authors that the life calculation based on ISO is qualitatively unreliable for pitch bearings.

In the following, the life calculation approach for three-row roller bearings is discussed. Section 2 discusses the FE simulation model used for this paper, and the ways in which it has been validated. Using this model, a grid of FE simulations was calculated for interpolation of all load cases of the turbine. The choice of this grid is discussed in Sect. 3. Section 4 then discusses how rolling contact fatigue life for individual load cases is calculated here and calculates it for the FE grid points from the previous section. Section 5 then finally covers how these results are processed to obtain a pitch bearing life representative of the entire turbine operational time. ~~Section ?? briefly discusses how this result can be put in relation to a fatigue test on a pitch bearing test rig.~~ Finally, Section 6 concludes the paper.

2 FE simulation

Accurate FE simulations are critical to a realistic life calculation. This section therefore covers the three-row roller bearing FE model including a short insight into the bearing validation process and the rotor FE model that was used to simulate the resulting load distribution for a variety of turbine load situations.

2.1 FE bearing model and validation

The three-row roller bearings implemented in the rotor model are created using the commercial ANSYS extension Rolling Bearing inside ANSYS (RBiA). The RBiA extension implements the rolling elements between the predefined raceway surfaces by COMBIN39 nonlinear spring elements that connect to the raceways by surface-based constraints. 21 springs are used to represent one ~~singe roller~~ single roller because this was the maximum possible amount of springs that could be used in the extension at the time of writing this paper. The force deflection curves of the nonlinear spring elements are calculated according to the defined curvatures of the ~~contact partners~~ contacting roller and raceway according to ISO ~~/TS~~ 16281. A crowning of the axial and radial rollers is considered according to the same standard. Furthermore, the bearing model considers clearance or preload of rows by means of PRETS179 elements. Negligible geometric details like small holes or lubrication channels are removed in order to enable a smoother mesh generation. High order tetrahedral elements with quadratic shape functions and mid nodes are used for the meshes of the bearing rings. As it is typical for three row roller bearings, one of the inner or outer rings splits up into two rings as it is necessary for the assembly process. The split may occur on the inner or outer ring, depending on the bearing design. In Fig. 1, it is located on the outer ring. The location of the split for the bearing in this paper is confidential, Fig. 1 is not necessarily representative. This split of the ring is considered in the model and the surfaces are connected to each other by an internal frictional contact. The blade bearing model was validated with measured strain data obtained from a real scale test on the BEAT6.1 test bench of the Fraunhofer IWES. This test bench tests two bearings simultaneously and applies the loads with six hydraulic actuators in hexapod configuration. Adapter components emulate the bearing's surrounding stiffnesses. Figure 2 shows the BEAT6.1 with an exemplary test setup for 5 m blade bearings. More information about the test environment can be taken from Stammler (2020). Strain gauges are attached equidistantly to the blade bearing's inner and outer ring as depicted in Fig. 3.

For the validation process, static tests were performed with pure bending moments. As the strain gauge signal fluctuates over time, the data is averaged over the time the applied load of the test bench is kept constant. Furthermore, according to the recommendation in Graßmann et al. (2023) for a blade bearing validation, in some tests the applied bending moment was kept constant while the blade bearing was pitched. The measured data of the different strain gauges is plotted against the simulated data for the maximum of the ramped loads. Whereas the measured data is only available at certain circumferential positions, the FE simulated data is postprocessed along the entire circumference via path operations considering a high number of sample points. Either the axial or the tangential strains are postprocessed depending on the path's position. Figure 4 shows the comparison of axial strain values for inner and outer ring at a high M_x bending moment whereas Fig. 5 shows the comparison for the tangential strain values.

Even if there are slight discrepancies at certain positions, the overall characteristics of the deformation behaviour match well between simulation and test. Figure 6 shows results for a constant M_y bending moment for the outer rings of both test bearings.

The scatter bars in the plots indicate the fluctuation in the measured signals which is caused by the pitch movements of the bearing. This finding was already described in Graßmann et al. (2023) in a more pronounced way for scaled blade bearings. It can be seen that the scatter bars due to the pitch movements can be differently pronounced between both test bearings.

Figure 2. BEAT6.1 test bench ©Fraunhofer IWES/Marcus Heine

However, the deviations between simulation and test are in the same range as the scatter caused by the pitch movements. One possible explanation for the slight deviations between simulation and test could be, that only the bearing bolted connections are considered in this stage of the BEAT6.1 FE model in order to save computational time. Later on, some investigations with different test assemblies have shown that test rig internal bolted connections can also affect the bearing strain results up to this extent. However, as the focus was on the validation of the bearing model and there is a good agreement between simulation and test results for the global deformation behaviour, it is assumed that with this bearing FE model realistic raceway deformation and tilting is simulated as well, which is crucial for the subsequent bearing lifetime calculations.

2.2 FE rotor model

Like the bearing FE model, the global FE rotor model is built up in the ANSYS workbench environment. The focus is put on accuracy and on efficiency of the model in order to be able to perform a high number of simulations in a reasonable time. The high number of simulations is required in order to evaluate the resulting bearing load distributions for a variety of different load situations required for the advanced subsequent lifetime calculations. The rotor model contains the rotor hub, three blade dummies, one blade bearing at the primary flange (1), two blade bearing dummies at the secondary flanges (2, 3) and bearing

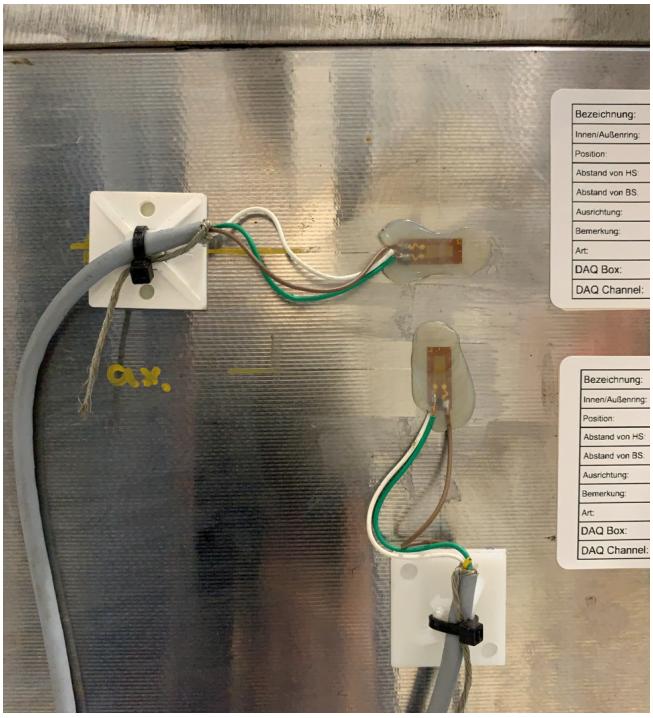

Figure 3. Strain gauges on the roller bearing's outer ring.

stiffening components at all three flanges. Figure 7 shows an exemplary FE rotor model which is built up in a comparable manner.

Only the blade dummies used for the present investigation are cylindrical and shorter as the blade structures depicted in Figure 7. The three blade dummies are meshed with a hex-dominant method to reduce the number of nodes and elements for these components. Bolted connections are considered only at the primary flange. They are implemented with BEAM elements that connect to washers which are modeled with 3D solid elements. The desired preload of both bolted connections is implemented with PRETS179 elements in the first load step. Only at the primary flange frictional contacts are considered between the component flange surfaces and for the contacts between component flange surface and washer surface. Different frictional coefficients are used depending on the flange surface individual coating. A general joint with the connection type "Body-Ground" is applied to the hub's rotor flange to fix the entire model and implement a certain stiffness to account for the rotor shaft. A so called "pitch lock" condition is implemented at the primary flange by means of a remote displacement. This boundary condition fixes only the nodal degrees of freedom in rotational z-direction and in turn prevents any rotatory displacements of the inner ring against the outer ring. As only the primary flange 1 is equipped with a full roller bearing model with spring elements no pitch lock boundary condition is necessary for the secondary flanges 2 and 3. The coordinate systems for the load application are shown in Figure 7. Forces and moments are applied to pilot nodes located in the centre of the blade dummy cutting plane at each flange. This lever arm between blade bearing flange and pilot node position is considered

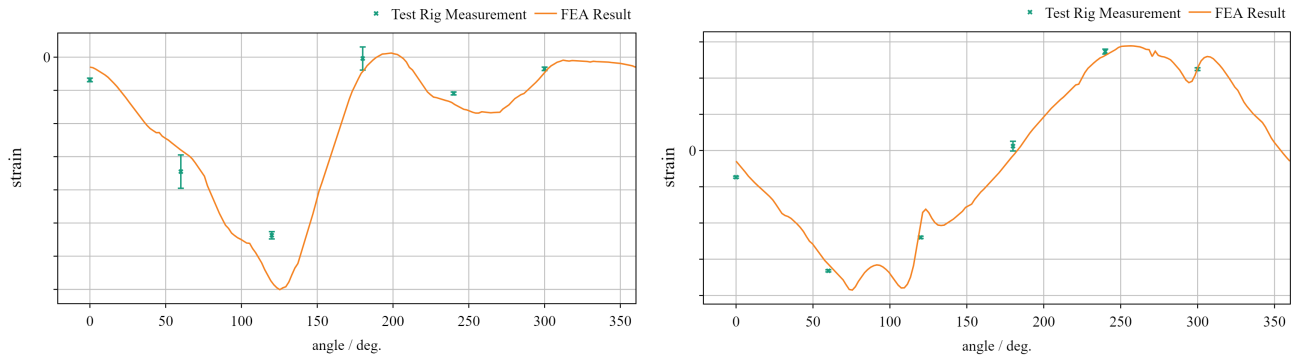

Figure 4. Axial strain for M_x bending moment for inner (left) and outer ring (right)

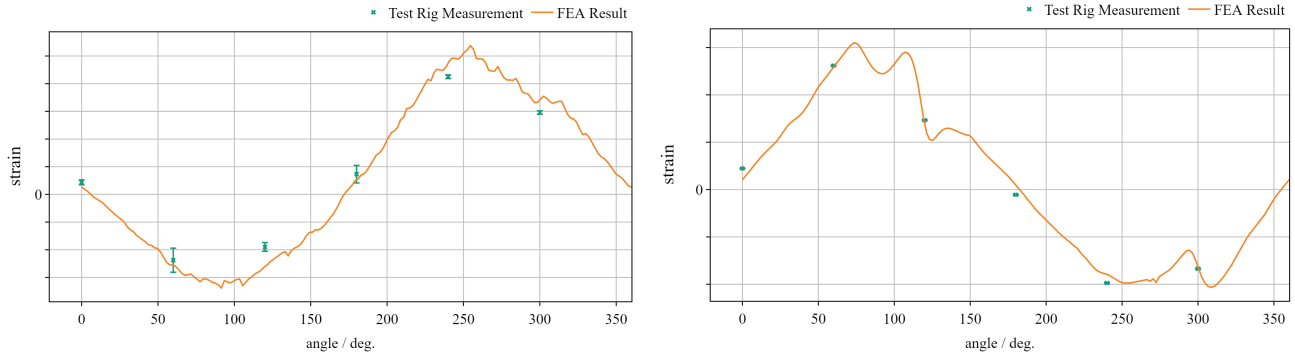

Figure 5. Tangential strain for M_x bending moment for inner (left) and outer ring (right)

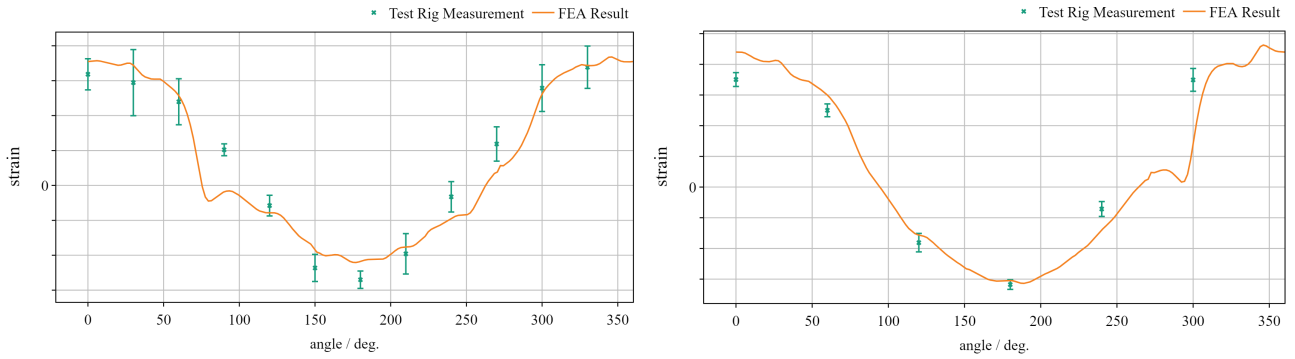

Figure 6. Outer ring tangential strain for M_y bending moment with pitch movement. Lower test bearing (left) and upper test bearing (right).

accordingly. Probe functions were used to verify the force and moment reaction at the blade bearing flange nodes. In addition, plausibility checks of the resulting load distributions were done for a variety of different load scenarios.

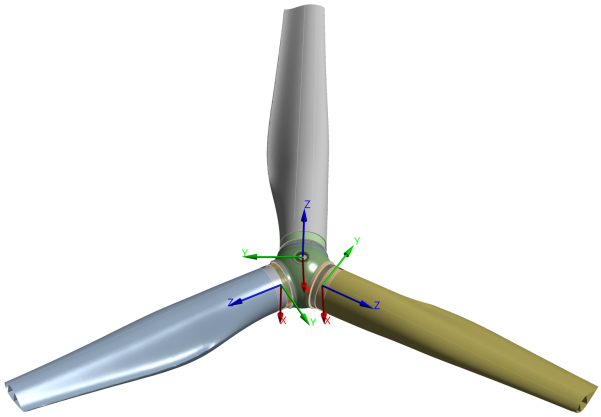

Figure 7. Exemplary FE rotor model of the IWT7.5 reference turbine.

3 FE simulation grid

Loads of the turbine have been calculated with aero-elastic simulations according to IEC 61400-1. Thus, there is a significant amount of time series simulation covering all power production (DLC 1.2), Fault (DLC 2.4), Start and Stops (DLC 3.1 and 4.1) and Parked conditions (DLC 6.4).

All time series were simulated using time steps of 50 ms. Taken together, these time series result in multiple millions of time steps. Post-processing these time steps into bins is a common approach to reduce the number of simulation points, used, for instance, in Schwack et al. (2016b); Menck et al. (2020); Keller and Guo (2022). However, using these time steps individually is more accurate than post-processing them into a smaller number of bins (Menck and Stammler, 2024). It is however practically impossible to calculate millions of FE simulations for the life calculation of a pitch bearing.

In order to be able to use individual time step data rather than using bins, a regression or interpolation akin to that shown in Menck et al. (2020) can be used. It is based on a reduced number of simulation points (hereafter referred to as "grid") that are simulated in FE. Contact forces or pressures of the bearing for aeroelastic loads in between these FE grid points are then determined via a regression or an interpolation.

There are 15 degrees of freedom (DOF) for the external loads in the FE model described in 2 (Note that the FE model obviously has far more internal DOF). They are F_x, F_y, F_z, M_x, and M_y for each of the three blades, respectively. Because the above described FE simulations need hours to run, this high number of DOF needs to be reduced down to a lower amount of DOF for the FE simulation grid.

The following sections describe the choice of FE grid points that will be used for interpolation in the following chapters, starting with the DOF for blade 1, which are most relevant for the load distribution in that bearing, and then continuing with the loads of blades 2 and 3.

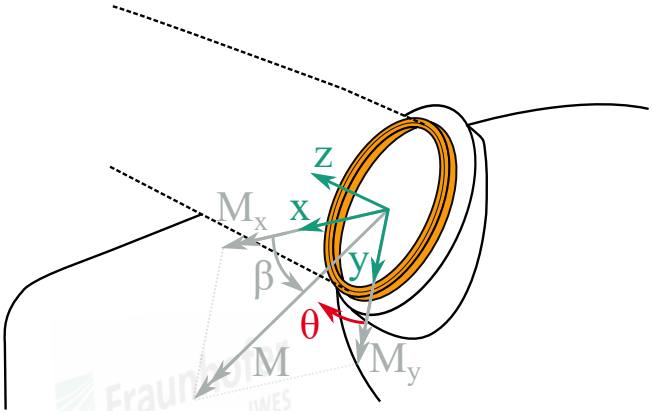

Figure 8. Coordinate system used for this paper, taken from Menck et al. (2020).

3.1 Degrees of freedom for blade 1

Pitch bearings experience significant loads in five degrees of freedom (DOF) according to the coordinate system in Fig. 8: F_x, F_y, F_z, M_x, and M_y. Since the sixth DOF (M_z) would be the rotational DOF of the bearing, it is comparatively small and can be neglected for the purposes of this paper. Aside from these DOF, the blade can also be rotated, which also influences the load distribution and can be considered as an additional DOF.

Previous publications by the authors have used the resulting bending moment M (also called M_{res}), the load angle β, and the pitch angle of the blade θ in order to define a grid of FE simulation points, see Menck et al. (2020). Further in-house analyses have shown that the influence of the pitch angle is relatively small in many turbines.

For these reasons, deviating from previous publications by the authors, the pitch angle was not used as a DOF in this paper. The resulting bending moment M and the load angle β (representing M_x and M_y) have continued to be included since they appear to be the most significant influence on the load distribution. This leaves the forces F_x, F_y and F_z to be somehow included in the FE simulations.

The following Sect. 3.1.1 will show that F_x and F_y are closely correlated with M_y and M_x and can thus be approximated based on them. F_z will be shown to correlate poorly with the bending moments and is thus included as additional DOF for the FE simulation grid. The Sect. 3.1.2 will then show that a very small number of F_z variations are required for the FE simulation grid.

3.1.1 Approximation of F_x and F_y for blade 1

Forces F_x and F_y are the resultants of weight and aerodynamic loads distributed over the entire blade length. They are a necessary input of the FE simulations. As the theoretical center point of the resultants changes with the distribution of the acting loads, they are not ideally correlated with the bending moments M_y and M_x at the blade root.

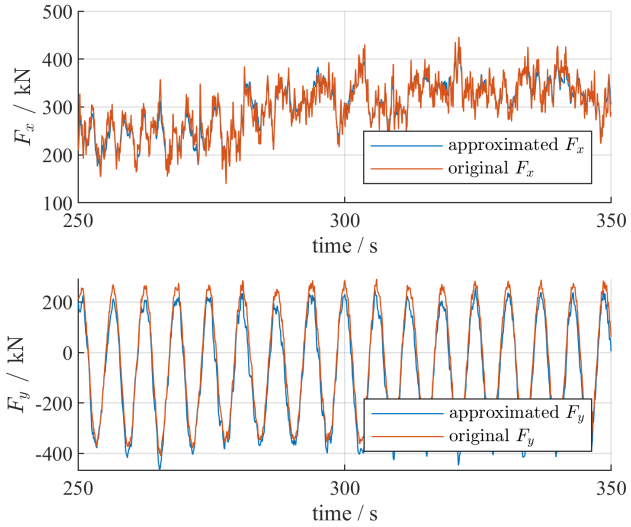

Figure 9. Approximations of F_x and F_y based on the bending moment, exemplary for IWT7.5

Despite this, there is still a close correlation between the blade root radial loads and bending moments. A linear approximation will be used here to approximate the radial loads based on the bending moment components chosen later in the FE simulation grid. To this end, all data points from the simulation were used to minimize the root mean square error (RMSE) of

$$F = a + M/b. \tag{1}$$

In order to be able to show detailed results, the authors also carried out this task using publicly available IWT7.5 aeroelastic data (Popko). Doing so resulted in

$$F_x = 63.06\,\text{kN} + M_y/56.61\,\text{m}, \text{ and} \tag{2}$$

$$F_y = 27.86\,\text{kN} - M_x/20.89\,\text{m}. \tag{3}$$

Over all simulation points of the IWT7.5 data, this resulted in an RMSE of 27.53 kN for the approximation of F_x via Eq. 2 and an RMSE of 51.08 kN for the approximation of F_y via Eq. 3. Figure 9 shows a sample section of a 12 m/s wind speed time series with the real aeroelastic F_x and F_y being compared to their approximations based on Eqs. 2 and 3. Qualitatively, the result can be seen to work well, and the RMSE of these methods is quite low compared to loads in operation, particularly for the more significant load component F_x which causes the flapwise bending moment M_y.

The same analysis was carried out using the aeroelastic data of the studied wind turbine and will be used for the FE simulations shown later. Attempts to correlate F_z with the bending moments ended poorly, with errors of a linear fit to the resulting bending moment being above 300 kN for the example IWT7.5 data shown above. For this reason, the axial load F_z was used as a third degree of freedom next to M and β.

3.1.2 Choice of grid simulation points for F_z for blade 1

The axial load is often considered as a linear factor for the approximation of rolling element loads, see Stammler et al. (2024). The authors of the present work hypothesized that two FE simulations at the upper and lower end of F_z might be sufficient to determine any other F_z load in between these extremes.

To verify this hypothesis, ten FE simulations were carried out using the models shown in Sect. 2: Five with varying levels of F_z for a relatively low bending moment in the lower 10 to 20 % of DLC 1.2 bending moments, and one in the upper 90 to 100 % thereof. The five levels of F_z are normalized to -0.33, 0, 0.33, 0.67, and 1 in this paper. Upper and lower end of F_z (i.e., $F_z = -0.33$ and 1) were close to actual upper and lower end seen in DLC 1.2. This resulted in load distributions for two axial rows and one radial row, all of which contained rollers that were discretized into 21 laminae for the FE simulation.

Roller lamina loads q of levels $F_z = 0, 0.33$, and 0.67 were then interpolated only using the FE load data from the extremes at $F_z = -0.33$ and 1. A linear interpolation was used. An excerpt of the result is shown in Fig. 10 for a lamina at the center of the roller and for an exemplary roller on Axial row 2. The lamina load q can be seen to be represented well using the interpolation, particularly at the top of the load distribution. Merely at the lower end, discrepancies are visible; these are, however, of exponentially smaller influence to the final rolling contact fatigue life.

Qualitatively, the result appeared the same for Axial row 1 and the radial row: Higher forces were interpolated very well, only at the lower end of the load distribution, the interpolation underestimated forces. Since ~~high forces~~ highly loaded rolling elements are those that affect the life the most, this result is adequate for the life calculation.

From examining these and more results of the simulations for various rollers and laminae, the authors conclude that it is valid to interpolate two extreme load levels of F_z and to interpolate in between them. This works particularly well for high lamina loads, which are the most relevant for rolling contact fatigue life.

3.2 FE simulation grid for blade 1

Concluding from the above discussed results, three degrees of freedom are sufficient for the FE simulation grid. These include bending moment M, load angle β, and axial load F_z. The loads F_x and F_y are strongly correlated with M_y and M_x and thus do not need to be considered separately. The pitch angle has a low influence, particularly for the given study, and is therefore negligible.

The bending moment's influence on roller lamina loads q is by far the biggest out of DOFs. However, it is also relatively linear in behavior. The load angle's influence is not as significant, but highly nonlinear. Therefore, a similar number of FE grid points were used for M and β. Based on previous experience, the authors opted for 6 points for M and 7 points for β, as well as two points for F_z due to the reasons discussed above. This results in $6 \cdot 7 \cdot 2 = 84$ FE simulations that will form the basis for all calculations in this paper. For illustrative purposes, the grid has been recreated using IWT7.5 data, shown in Fig. 11.

It can be seen that no FE simulations were carried out in the range of $\beta = 0 ... -180°$. This is because this range represents very rare operating points which have little significance on life. The studied wind turbine data included even fewer points than the IWT7.5 shown in Fig. 11, making this choice even more appropriate. The grid shown in Fig. 11 also contains 14 FE

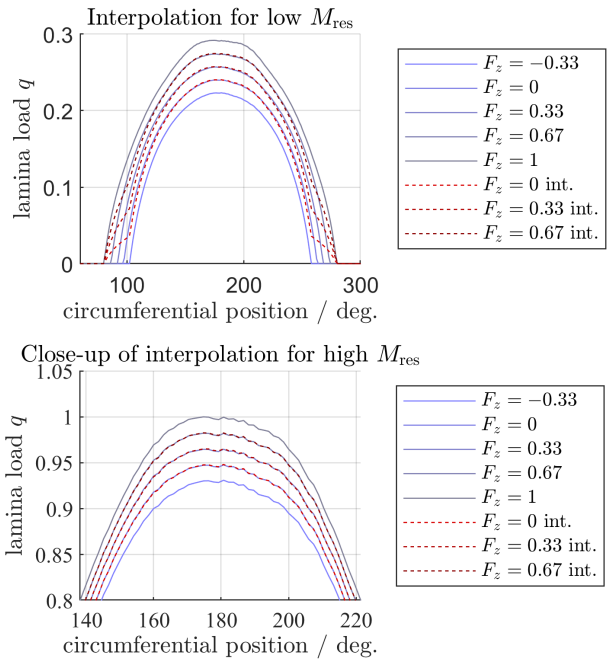

Figure 10. Interpolation of simulations with varying F_z. Center lamina load on Axial row 2. Lamina loads q normalized to maximum load in the figure. F_z normalized to maximum load for the present study.

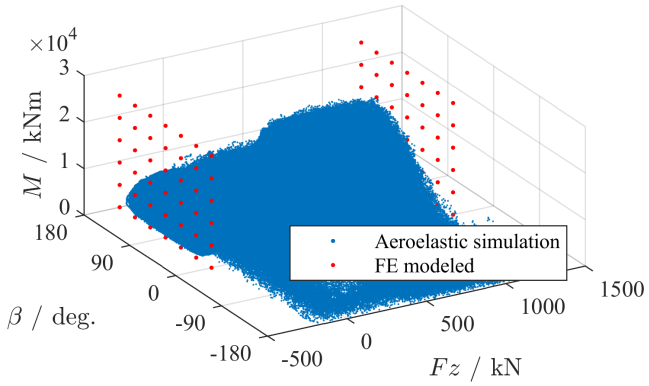

Figure 11. Grid of FE simulations vs. aeroelastic time steps, exemplary for IWT7.5

simulation points at a bending moment of $M = 0$, in which case the load angle is irrelevant; thus, only two of these simulations have been carried out for the high and low F_z load each. Therefore, only 72 FE simulations were actually carried out. Tables A1 and A2 contain the grid data points that were simulated, where moments have been given depending on the maximum bending moment $M_{\max}$ that was simulated here, and only the sign (positive or negative) is given for F_z.

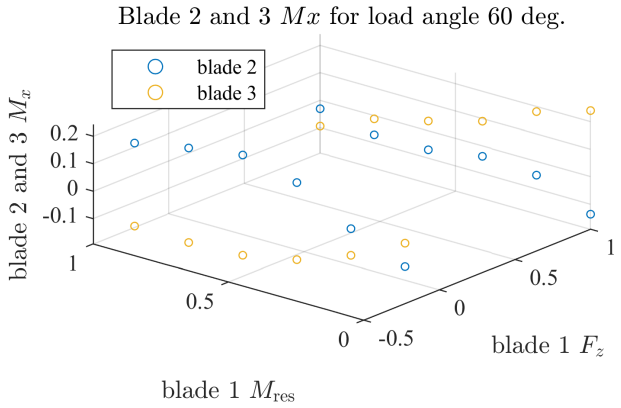

Figure 12. M_x of blades 2 and 3 depending on M_{res} and F_z of blade 1 for studied turbine. Axes normalized to maximum M_{res} and F_z.

3.3 Loads at blades 2 and 3

The FE model used in this paper is a full rotor model and thus also requires loads at blades 2 and 3. These influence the load distribution in the bearing, especially at circumferential positions close to other bearings, and therefore need to be determined for the simulation grid used here (Schleich et al., 2024).

In principle, this adds another 3 DOF for each of the other two blades; however, while they have a minor influence on RCF calculation results, it does not justify such a huge increase in computational expense for the scope of the present work (Note this influence of blade 2 and 3 is likely more significant for other damage modes such as ring cracks, as they influence the edgewise loads, which are known to affect ring cracks (Becker and Jorgensen, 2023)). For pragmatical purposes and because previous analyses determined that there is some influence of the other two blades, but it is less critical than that of the first blade, mean values of blades 2 and 3 were determined for the grid shown in Fig. 11. In Stammler and Schleich (2024), similar mean values are determined. While the present work uses F_z, Stammler and Schleich (2024) use the rotor azimuth angle $\Phi_{\mathrm{r,B}}$. Standard deviations for the approach used in the present work have not been determined as the influences of blade 2 and 3 on blade 1 are less critical than in the case of a structural fatigue calculation as in Stammler and Schleich (2024).

An excerpt of these results is shown in Fig. 12, where some average values for M_x of blades 2 and 3 are shown based on the blade 1 loads in the FE simulation grid, and in Fig. 13, where the values of M_y of blades 2 and 3 are shown.

M_y of blades 2 and 3 can be seen to be correlated well with blade 1, which is plausible, since all of them are loaded similarly by the wind. The correlation between M_x of blades 2 and 3 with the blade 1 loads is more complex, but still plausible: At negative values of F_z, blade 1 points upward. This means blade 2 is generally experiencing a positive M_x, since it is located 120 degrees further in rotational position of the hub, where gravity is acting in its positive M_x direction, and blade 3 is experiencing a negative M_x since it is located yet another 120 degrees further, where gravity is acting in the negative M_x direction. For cases of high postive F_z values, the situation is opposite, and blade 1 pointing downwards means that blade 2 is experiencing a negative M_x due to gravity whereas blade 3 a positive one.

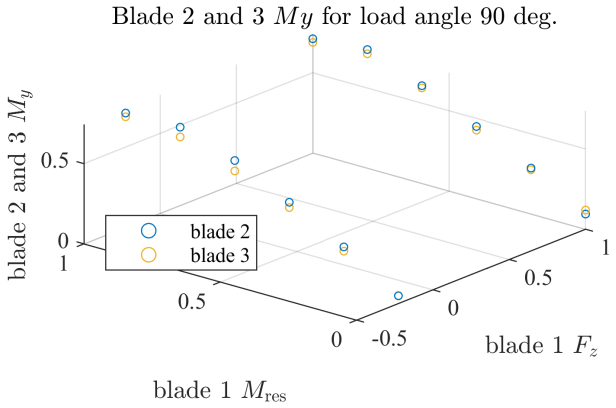

Figure 13. M_y of blades 2 and 3 depending on M_{res} and F_z of blade 1 for studied turbine. Axes normalized to maximum M_{res} and F_z.

4 Rolling contact fatigue life for individual load cases

The rolling contact fatigue life calculation adheres closely to the ISO/TS 16281 based methodology described in NREL DG03 (Stammler et al., 2024)~~and, in turn, ISO/TS 16281.~~. These documents far exceed the requirements of a more simple life calculation according to ISO 281. They require a detailed pressure distribution coming from a detailed simulation of the bearing that includes rollers divided into several laminae. As described above, this aim is achieved here by usage of FE simulations. The result of this calculation is then, according to the abovementioned documents, processed with a non-Hertzian contact calculation. The non-Hertzian pressure distribution is then used to calculate the life of each raceway which are then combined to obtain a total life.

This section covers the calculation for individual load cases obtained from FE in order to carry out various analyses and checks prior to the calculation of the ~~operational~~ fatigue life of the bearing. The calculation procedure for bearing life L_{10} is given in Sect. 4.1. This calculation requires contact pressures, the calculation of which is discussed in Sect. 4.2. Finally, the life of the grid of FE simulations from Sect. 3 is calculated in Sect. 4.3.

4.1 Calculation of L_{10}

The L_{10} life for calculations in this section were calculated according to the NREL DG03 (Stammler et al., 2024) which closely adheres to ISO/TS ~~16281.~~ 16281 (now ISO 16281). According to NREL DG03, the bearing is separated into two axial rows and a radial row.

The axial row calculation starts with the determination of their load rating C_{a}, which is identical for both axial rows, as

$$C_{\mathrm{a}} = b_{\mathrm{m}}\, f_{\mathrm{c}}\, L_{\mathrm{we}}^{7/9}\, Z^{3/4}\, D_{\mathrm{we}}^{29/27} \tag{4}$$

where $b_m = 1$, L_{we} is the effective roller length (i.e., roller length minus chamfer), Z is the number of rollers per axial row, and D_{we} is the roller diameter. The variable f_{c} is calculated according to ISO/TR 1281-1.

For the radial roller row, the load rating C_r is calculated as

$$C_\mathrm{r} = b_\mathrm{m}\, f_\mathrm{c}\, (L_\mathrm{we} \cos\alpha)^{7/9}\, Z^{3/4}\, D_\mathrm{we}^{29/27} \tag{5}$$

where α is the nominal contact angle of $0°$ for the radial row, and $b_m = 1.1$ for the radial roller row.

Using these load ratings, the variables Q_ci and Q_ce for the inner and outer ring are determined. For the axial rows, these are identical due to the $90°$ contact angle, giving

$$Q_\mathrm{ci} = Q_\mathrm{ce} = \frac{1}{\lambda\nu}\frac{C_\mathrm{a}}{Z} 2^{2/9} \tag{6}$$

where $\lambda\nu = 0.73$ for the axial row.

For the radial row, they are given by

$$Q_\mathrm{ci} = \frac{1}{\lambda\nu}\frac{C_\mathrm{r}}{0.378\cdot\, Z\,(\cos\alpha)\, i^{7/9}} \left\{ 1 + \left[1.038 \left(\frac{1-\gamma}{1+\gamma} \right)^{143/108} \right]^{9/2} \right\}^{2/9} \tag{7}$$

$$Q_\mathrm{ce} = \frac{1}{\lambda\nu}\frac{C_\mathrm{r}}{0.364\cdot\, Z\,(\cos\alpha)\, i^{7/9}} \left\{ 1 + \left[1.038 \left(\frac{1-\gamma}{1+\gamma} \right)^{143/108} \right]^{-9/2} \right\}^{2/9} \tag{8}$$

where $\lambda\nu = 0.83$ for the radial row and $\gamma = D_\mathrm{w}\, \cos\alpha / D_\mathrm{pw}$.

From now on, the equations are identical for axial and radial row, though results will differ due to the different dimensions of the rows and their rollers.

The basic dynamic load ratings q_ci and q_ce of a lamina for inner and outer ring are given by

$$q_\mathrm{ci/e} = Q_\mathrm{ci/e} \left(\frac{1}{n_\mathrm{s}} \right)^{7/9} \tag{9}$$

where n_s is the number of laminae (sometimes also called slices) into which the roller is divided for the calculation. Equation 9 assumes laminae of even length. In Sect. 4.2.1, a convergence analysis is carried out in order to determine the amount of laminae used for the remainder of this paper.

Potentially occurring edge stresses are accounted for by use of a non-Hertzian model that is described in Sect. 4.2. For each roller j and lamina k, the stress riser functions $f_\mathrm{i}[j,k]$ and $f_\mathrm{e}[j,k]$ for the inner and outer rings are given by

$$f_\mathrm{i/e}[j,k] = \left[\left(\frac{p_\mathrm{Hi/e},j,k}{271} \right)^2 D_\mathrm{we}\, (1 \mp \gamma)\, \frac{L_\mathrm{we}}{n_\mathrm{s}} \right] / q_{j,k} \tag{10}$$

where p_Hi,j,k and p_He,j,k are the pressures on lamina k of roller j, determined using the non-Hertzian model described in Sect. 4.2, for inner and outer ring, respectively.

The dynamic equivalent load for each lamina k can now be calculated. Following NREL DG03 and Menck and Stammler (2024), the equivalent load for a stationary ring is used for both inner and outer ring, since pitch bearings oscillate by relatively small amplitudes. These small oscillations cause the oscillating ring to be almost stationary w.r.t. the load, differing from a

rotating bearing, where the rotating ring rotates relative to the load. Thus, for all raceways,

$$q_{k\mathrm{ei/e}} = \left[\frac{1}{Z} \sum_{j=1}^{Z} \left(f_{\mathrm{i/e}}[j,k]\, q_{j,k} \right)^{4.5} \right]^{1/4.5} \tag{11}$$

Note that when Eq. 10 is put into Eq. 11, the lamina load $q_{j,k}$ cancels out and is therefore not actually required for the life calculation.

The life of each inner-outer raceway pair m, i.e. of the first axial row ($m = 1$), the second axial row ($m = 2$), and the radial row ($m = 3$), is then given by

$$L_{10\mathrm{r},m} = \left\{ \sum_{k=1}^{n_\mathrm{s}} \left[\left(\frac{q_{k\mathrm{ci}}}{q_{k\mathrm{ei}}} \right)^{-4.5} + \left(\frac{q_{k\mathrm{ce}}}{q_{k\mathrm{ee}}} \right)^{-4.5} \right] \right\}^{-8/9} \tag{12}$$

Finally the life of the entire bearing is calculated using

$$L_{10} = \left(\sum_{m=1}^{3} L_{10\mathrm{r},m}^{-9/8} \right)^{-8/9} \tag{13}$$

Up until this point, the life is measured in millions of revolutions. Consideration of the oscillatory behavior of pitch bearings will follow in Sect. 5.2.

4.2 Contact pressure calculations

The FE simulations are carried out using 21 laminae, resulting in 21 lamina loads $q_{\mathrm{FE},k}$ for each roller j. ~~The~~ Pressures of these laminae can be calculated using Hertzian theory. However, Hertzian theory simplifies the roller-race contact and may underestimate the real pressure. Therefore, the resulting load and moment from these laminae are then determined for each roller j according to

$$Q_j = \sum_{k}^{21} q_{\mathrm{FE},j,k}, \tag{14}$$

$$M_j = \sum_{k}^{21} t_k \cdot q_{\mathrm{FE},j,k}, \tag{15}$$

where t_k is the distance of the center of lamina k from the roller center. Since M_j is the moment around the roller center, t_k assumes negative values in negative direction and positive ones in positive direction. The force and moment are then used as an input to an adapted non-Hertzian contact calculation based on Reusner (1977). This returns a more accurate ~~load~~ pressure distribution than the FE simulation and is capable of accurately detecting edge stresses that may occur in a roller and that would go unnoticed by FE simulations using the approach described in Sect. 2. Reusner proposed an approach that determines contact properties such as roller force, moment, pressure, and contact width based on the displacement and misalignment of the roller. The calculation by Reusner has been chosen because it is one of three methods that are explicitly suggested for this task by ISO ~~/TS~~ 16281 and NREL DG03. It has been adapted for this paper in order to use forces and moments as input rather than as outputs, referred to as “inverted Reusner calculation” (or just “Reusner” for short) in the following.

4.2.1 Contact convergence analysis

For the non-Hertzian contact calculation according to Reusner (1977), the roller is evenly discretized along its length into n_s laminae. The number of laminae for the FE simulation and the inverted Reusner model are unrelated and can be chosen completely independently. The amount of laminae to perform an accurate life calculation depends on the specifics of the loading that the rolling bodies are experiencing, and on the roller design, including its profile. Particularly the occurrence of edge loading or strong misalignment necessitates a higher number of laminae.

In order to determine the required amount of laminae per roller for the following life calculation, convergence analyses were carried out with the inverted Reusner calculation. To this end, the rollers were divided into n_s laminae of even length. The variable n_s was varied from ten to 100 in steps of ten, and then additionally once set to 150. Life of the raceways and the entire bearing were determined according to Sect. 4.1 for each of the different values of n_s. The roller life at $n_\mathrm{s} = 150$ was used as a reference for the lives at lower lamina numbers.

The convergence analysis showed that the axial raceway 1 (near the blade flange) and the radial raceway both converged well. With 30 laminae, these raceways already converged within 3 % error of the final reference result at 150 laminae, with the exception of a single simulation for the first axial raceway. The second axial raceway (near the hub) converged more poorly. 8 of the 72 simulations did not yet reach less than 3 % of difference compared to the reference result at 150 laminae using 30 laminae. These are, however, mostly unrealistic load situations that are used for interpolation purposes at rare operating points only.

However, only the life of the entire bearing and its convergence really counts for the further calculations. For the life of the entire bearing and using 30 laminae, only 5 of the 72 simulations (Nr. 10, 20, 62, 71, 72) did not reach a life within 3 % of the reference result at 150 laminae. All of these five load situations represent unrealistically high cases of mostly edgewise bending moments that do not occur in reality and are only used for interpolation of rare operating points. All other simulations were within 3 % difference of the reference when using 30 laminae. Figure 14 shows results of the convergence analysis for simulation nr. 36, 38, 40, and 42. These correspond to pure flapwise bending moments with a positive F_z and 40 %, 60 %, 80 %, and 100 % of M_max, respectively, see tables A1 and A2. The convergence behavior can be seen to deviate from the reference for higher lamina numbers (for instance $n = 70$ for sim. nr. 42) and then to converge towards the reference. This is due to edge stresses that occur in some contacts of the Reusner calculation for the particular calculations done in this paper with a medium amount of laminae, and it shows why a convergence analysis is necessary.

Pressure distributions for sim. nr. 42 (maximum M_res load case, pure flapwise direction, positive F_z) are given in Fig. 15. All rollers of each raceway are shown and plotted on top of each other. For the axial raceways, inner and outer ring pressures are identical due to the contact angle of $\alpha = 90°$. For the radial rollers, inner ring pressures are displayed. While there is some misalignment present on all raceways, its effect is most significant on the axial raceway 2. Maximum loads all occur at the highest bending moment M_max that has been simulated, but for different load angles thereof. As shown above in Fig. 11, M_max represents a very rare load situation during operation, and the overall highest pressures occur at load angles that do not occur in operation for such high loads. These simulations and are only used for interpolation of rare operating points.

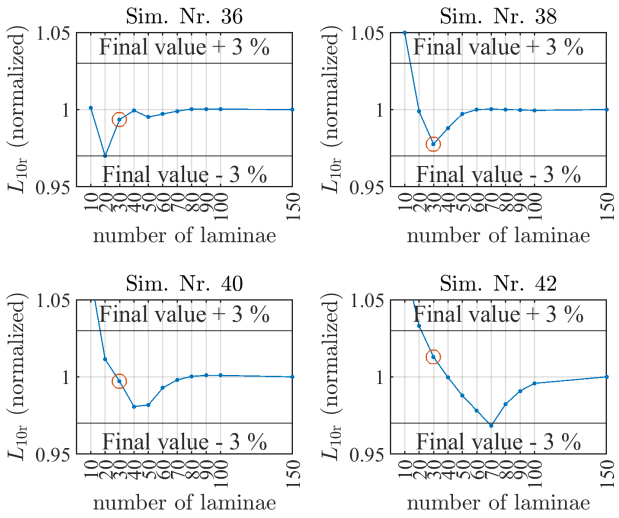

Figure 14. convergence analysis of L_{10r} for selected FE simulations (see tables A1 and A2). Result for $n_s = 30$ laminae marked red.

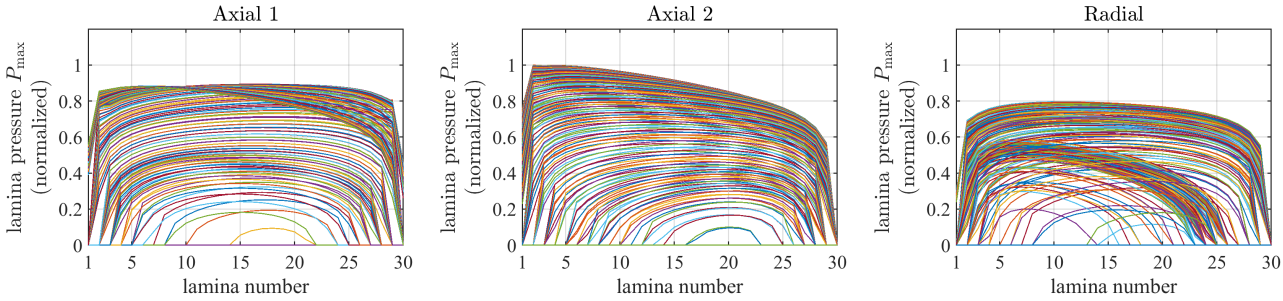

Figure 15. Pressure distributions of all rollers on axial raceway 1, 2, and radial raceway. Obtained via inverted Reusner algorithm. Simulation nr. 42 (M_{max}, $+F_z$, and $\beta = 90$). Pressures normalized to maximum pressure within the three figures.

The pressures that have been obtained via the inverted Reusner algorithm can be compared to those directly obtained from FE using a lamina approach as described in Sect. 2. A comparison of both pressure results is given in Fig. 16. The center of the roller can be seen to have slightly higher results than the results directly obtained via FE (0.9 % higher for both axial rows and 0.5% for the radial row). Conversely, towards the edges of the roller, the FE results have much higher pressures, since the Reusner processed results decrease strongly at the outer ends (see Fig. 15) whereas the FE results barely decrease at all at the edges.

In any case, both results are very similar. This is due to the identical profiles used both in FE as well as the inverted Reusner algorithm, as well as because of the fact that no edge pressures occur. A non-Hertzian analysis for the roller pressures is particularly necessary because edge pressure spikes can occur with an unsuitable choice of profile or if there is a lot of roller misalignment. In the present case, there are no edge pressure spikes present. Therefore, the results are similar to the FE results.

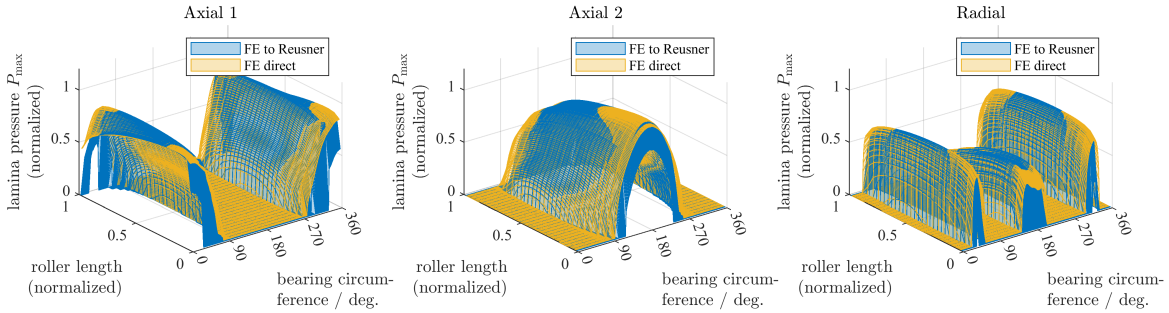

Figure 16. Pressure distribution of all rollers on axial raceway 1, 2, and radial raceway, directly obtained from FE as well as post-processed via inverted Reusner algorithm. Simulation nr. 42 ($M_{\max}$, $+F_z$, and $\beta = 90$). Pressures normalized to maximum pressure of Reusner processed results within the three figures.

Had the profile been less adequate, or if there had been more misalignment, there would be more deviations between the two approaches.

4.3 Bearing life of FE simulated cases

The lives $L_{10\mathrm{r}}$ of all 72 simulations have been calculated according to the above equations. They are shown in Fig. 17. While all further calculations will use $L_{10\mathrm{r}}$ with inverted Reusner post-processing, $L_{10\mathrm{r}}$ without it, using the Hertzian pressure from FE, has also been calculated for reference. Life $L_{10\mathrm{r}}$ has been normalized to the maximum $L_{10\mathrm{r}}$ obtained with the inverted Reusner post-processing approach.

The results of both approaches can be seen to be very similar, which is due to the fact that both approaches lead to similar pressure distributions in this study, see Fig. 16 and the corresponding discussion. The lowest $L_{10\mathrm{r}}$ lives in Fig. 17 correspond to the highest bending moments, see Tables A1 and A2. An increase in F_z appears to have a positive effect on $L_{10\mathrm{r}}$ for some simulations and a negative one on others. Further, the load angle β appears to have a small but noticeable effect, with the simulations at $\beta = 90°$ deviating the most from the other load angles that were simulated. Because pre-tension in the bearing was considered, the rollers were loaded even at $M_{\mathrm{res}} = 0\,\mathrm{Nm}$ (Simulation Nr. 21 and 32) and thus a finite life $L_{10\mathrm{r}}$ is obtained even for these simulations.

Fig. 18 shows the lives $L_{10\mathrm{r}}$ of all three raceways separately, normalized to the highest $L_{10\mathrm{r}}$ among the axial rows, i.e., the life of Axial 1 in simulation 32. The radial row has the highest life $L_{10\mathrm{r}}$ out of all three raceways, with few exceptions for some simulations. Both Axial row 1 and the radial row appear to benefit from an increase in axial force F_z, while $L_{10\mathrm{r}}$ of Axial row 2 decreases with an increase in F_z. The whole bearing life is most affected by those raceways with a low $L_{10\mathrm{r}}$, see Eq. 13. Especially at the high bending moment load cases in which the total life is lowest, the whole bearing life can thus be seen to be dominated by the axial rows whose life is much smaller than that of the radial row.

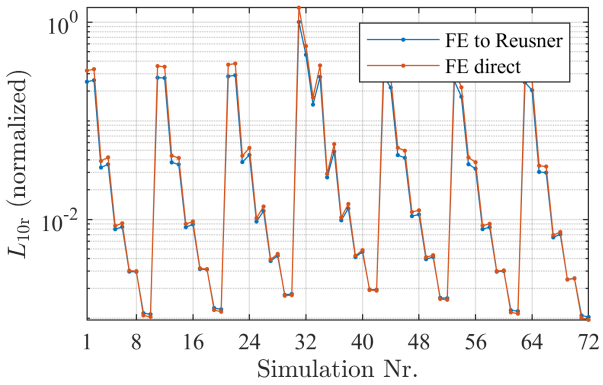

Figure 17. L_{10r} of all 72 FE simulations, normalized. Results shown for FE results with and without inverted Reusner post-processing.

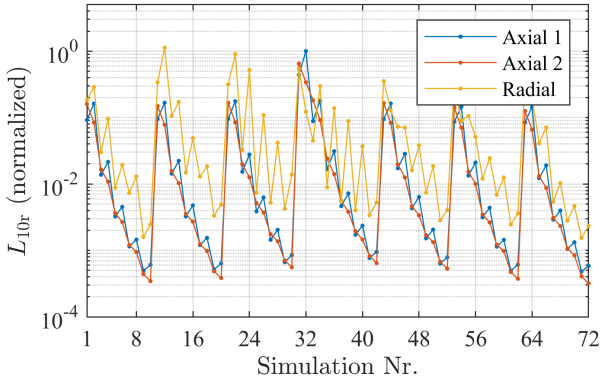

Figure 18. L_{10r} of all raceways of all 72 FE simulations, normalized.

5 Rolling contact fatigue life for the entire operating time

In this section, the life of the bearing under all operating conditions that it experiences is calculated. To this end, the contact pressures in each time step of the simulation are determined. The procedure to determine contact pressures for any time step is described and tested with sample simulations in Sect. 5.1. Section 5.2 then discusses how the lives of all time steps are combined into one total operating life. Finally, Sect. 5.3 proposes a simplified method for the life calculation of a three-row roller bearing based on the previously achieved results.

5.1 Interpolation of pressures

The grid chosen in Sect. 3 was based on a previous publication by the authors (Menck et al., 2020) in which contact forces were determined using a regression for a double-row four-point bearing. For the present roller bearings, pressures are required

rather than forces (loads). This is because the lamina load $q_{j,k}$ cancels out when Eq. 10 is put into Eq. 11, but the pressure $p_{\mathrm{Hi/e},j,k}$ does not cancel out.

Using a regression or interpolation of forces is a likely feasible approach since contact forces are roughly proportional to the bending moment M in particular, which has the highest influence on rolling element loads (Stammler et al., 2024). However, for the present roller bearing calculation, contact forces from FE must be postprocessed into an inverted Reusner algorithm, see Sect. 4.2. While the inverted Reusner algorithm is much faster than an FE simulation, it takes some seconds (approximately 30 seconds for one load case in this paper on a standard business laptop) to calculate an entire bearing load case with $n_{\mathrm{s}} = 30$ laminae as used in this paper, because there are hundreds of contacts in the bearing that need to be simulated.

Based on Menck and Stammler (2024), a calculation in which time steps are directly used as input is more accurate than one where post-processing of the time steps into bins takes place. Therefore, usage of time steps is the preferred choice that will be used in this paper. However, with multiple millions of time steps taken from the aeroelastic simulations for this paper (see Sect. 3), a computation with the inverted Reusner algorithm for every single step becomes too computationally expensive.

While contact force and contact pressure in a rolling bearing are not proportional, they can locally be approximated as linear. Therefore, a regression or interpolation of the pressures is a more feasible alternative to the computationally heavy and long-enduring alternative in which roller forces are interpolated (or determined via a regression) and must be processed with a non-Hertzian calculation for each time step.

Thus, instead of interpolating (or approximating via a regression) forces, pressures will be interpolated (or approximated via a regression) in the following. To this end, the grid of FE simulations is processed through the inverted Reusner algorithm to obtain a pressure distribution for $n_{\mathrm{s}} = 30$ laminae, based on the results in Sect. 4.2.1. The pressure in each of these 30 laminae for each roller is then interpolated (or approximated via a regression) for each time step. The approach is tested in the following using randomly selected test cases. Different approximation methods - a regression and two interpolations - are compared.

5.1.1 Testing the interpolation

In order to verify the interpolation approach described above, 20 test simulations were carried out. They were actual operating points from the aeroelastic simulations, randomly sampled from wind speeds between 10 and 14 m/s. The test simulations were simulated including all 15 DOF, i.e., all 5 DOF of each rotor blade, and no simplification of DOFs akin to Sect. 3 has been undertaken for these 20 test simulations.

The life of these test simulations was then calculated by processing the results into the inverted Reusner algorithm and calculating the life using the above described procedure.

Then, for verification of the interpolation, the interpolation was applied to these test simulations. Their load angle, M, and F_z values were determined and the load distribution of these simulations was calculated. The location of the test simulations within the grid is given in Fig. 19 and Table B1. The life was then determined according to the above described procedure using the interpolated pressure distributions.

Three different approaches were used: A regression from Menck et al. (2020), a linear interpolation, and a cubic spline interpolation. The results are shown in Fig. 20. Lives are normalized to the highest life of the whole bearing using the FE

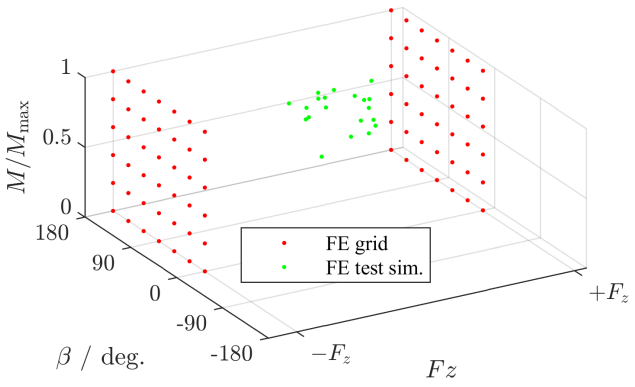

Figure 19. Locations of test simulations in FE simulation grid.

Table 1. Mean absolute percentage error of different approximation approaches compared to inverted Reusner post-processed FE results

Method	Total bearing	Axial 1	Axial 2	Radial
regression	18.64 %	19.63 %	12.88 %	371.73 %
linear int.	26.30 %	16.28 %	11.77 %	235.90 %
spline int.	13.71 %	4.91 %	2.93 %	193.56 %

results without interpolation or regression (”FE to Reusner”). Percentage errors (PE) were calculated for all 20 cases according to

$$\mathrm{PE} = \frac{L_{10,\mathrm{r,approx}} - L_{10,\mathrm{r,FE}}}{L_{10,\mathrm{r,FE}}} \cdot 100\% \tag{16}$$

Further, the mean absolute percentage error (MAPE) of these 20 cases was calculated as

$$\mathrm{MAPE} = \frac{1}{20} \sum_{i}^{20} |\ \mathrm{PE_i}\ | \tag{17}$$

and is shown in Table 1.

Out of all three approaches, the spline interpolation works best for rows Axial 1 and Axial 2, producing 4.91% error for Axial 1 and 2.93% for Axial 2 on average. The spline interpolation likely works better than the linear interpolation in particular because in this paper, pressures were interpolated. As discussed above, pressures and force are, however, not linearly correlated but slightly nonlinear. This nonlinearity is likely captured better by the spline interpolation. This is also visible by looking at the percentage error of the linear interpolation, which is almost always positive, because the linear interpolation underestimates the actual pressure due to the pressure’s nonlinearity, therefore overestimating the life. Further, the deformation behavior of the surrounding structures influence the load distribution and cause non-linear behavior w.r.t the moment M, which can be captured better with the spline interpolation.

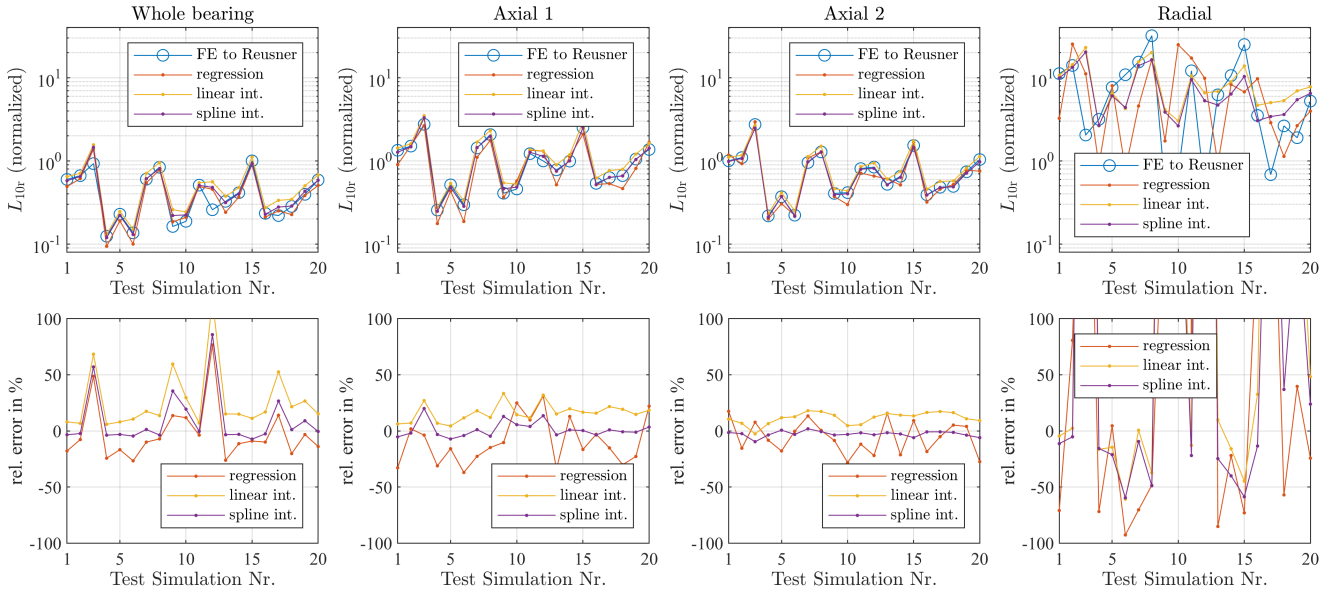

Figure 20. Top row: L_{10r} of all 20 test simulations, normalized, FE and interpolated. Bottom row: Percentage error for different approaches.

The interpolated pressures of Axial rows 1 and 2 are shown in Fig. 21 for test simulation 3. For this case, the errors for L_{10r} of Axial 1 are 3.2 % and those for Axial 2 are 3.6 %. The interpolated distribution can be seen to match the FE reference closely. Slight differences even out in the calculation of L_{10r}.

For the radial row, accurate results are not achieved with any of the methods. Even using the spline interpolation, deviations of over 190 % exist on average for the interpolated life of the radial row. However, because the radial row makes up only a relatively small portion of the total bearing life, the spline approximation of the total bearing life achieves only 13.71 % deviation on average, even despite the poor performance with respect to radial row life interpolation.

Analyzing the 20 cases here showed that even small deviations in bending moment M and load angle β away from the grid points can result in very large qualitative and quantitative changes of the pressure (and force) distribution in the radial row. An example case is shown in Fig. 22, where a test simulation and two grid simulations are plotted. The test simulation is number 3 from Table B1, whose interpolation results in very poor results, see Fig. 20. The simulation has a load angle of $\beta = 62.5°$ and a bending moment of $M = 0.4376 \cdot M_{\max}$. Both of these values are very close to the also displayed grid simulations number 23 and 24, both of which have load angle $\beta = 60°$ and $M = 0.4 \cdot M_{\max}$. The F_z value of test simulation 3 lies in between the extremes $-F_z$ and $+F_z$ from grid simulation 23 and 24, respectively. Despite this similarity, test simulation 3 can be seen to have higher pressures than either grid simulation 23 or 24. Aside from these quantitative differences, even the qualitative behavior is different, with grid simulation 24 carrying load at 0° and 90° where the other two simulations are carrying none, but carrying almost none at 180° where the other two are carrying a lot. Since the influence of F_z was checked in Sect. 3.1.2, it is unlikely that nonlinear behavior of the pressure in between the extremes of F_z explains this behavior.

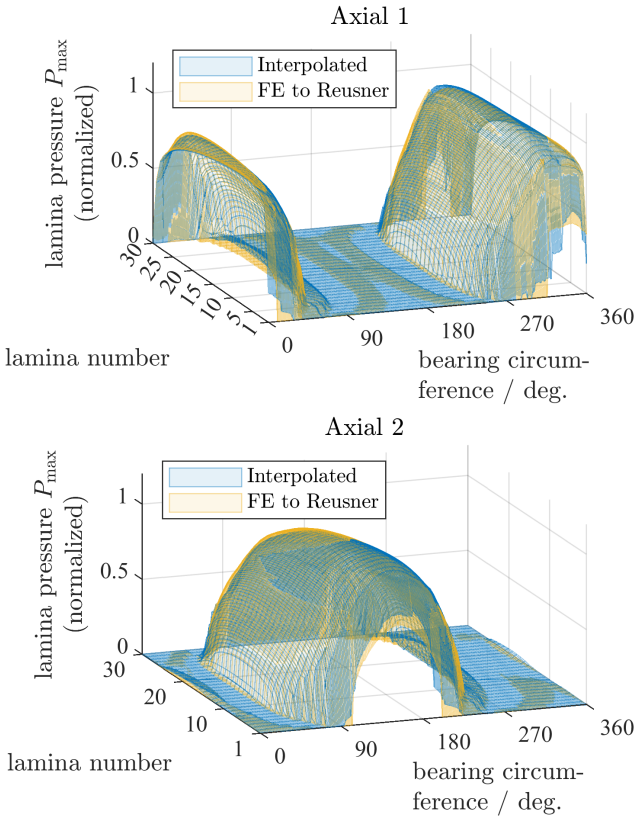

Figure 21. Test simulation 4: Interpolated pressure distribution vs. FE to inverted Reusner processed pressure distribution. Pressures normalized to maximum pressure of Reusner processed results of test simulation 4.

This indicates that the reason the radial row cannot be interpolated well may be due to insufficient available data for an accurate interpolation, that is to say, the radial row may be affected by more DOF than just those three used in this study. As discussed in Sect. 3, the grid was used based on a previous publication (Menck et al., 2020) that has been performed for a four-point bearing, which does not contain a radial row. The validity of F_z-based interpolation was explored in Sect. 3.1.2 and appeared to work well, but for more complex cases in which more than one DOF varies, the deformation may correlate worse with the three DOF chosen here. Ultimately, the pressure (and force) distribution that occurs in the radial row is very difficult to predict. To the current knowledge of the authors, it does not simply correlate with few DOFs but rather depends on the structural deformation of the entire bearing, which is affected by the interplay of all DOFs and the structural stiffness of the bearing.

The radial row therefore presents unfortunate properties:

- it makes up only a small portion of the total bearing life
- its calculation is very computationally expensive, because it contains a lot of rollers, and the inner and outer ring pressures are different and both have to be calculated

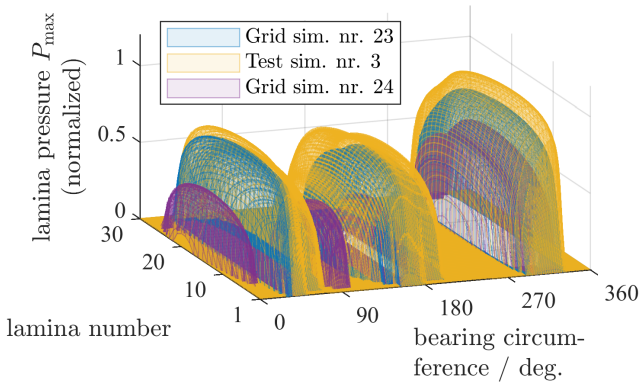

Figure 22. Radial pressures for grid simulation nr. 23 ($\beta = 60°$, $M = 0.4 \cdot M_{\max}$, $-F_z$), test simulation nr. 3 ($\beta = 62.5°$, $M = 0.4376 \cdot M_{\max}$, $+F_z \cdot 0.4294$), grid simulation nr. 24 ($\beta = 60°$, $M = 0.4 \cdot M_{\max}$, $+F_z$). These three cases highlight the difficulties in interpolating the radial row pressures, since test sim. 3 is close to grid simulations 23 and 24 w.r.t M and β and in between them w.r.t F_z, yet exceeds their pressures in many locations. Pressures normalized to maximum pressure of radial row in test simulation 3.

- its pressure (force) distribution is very difficult to predict and behaves in a very nonlinear fashion with respect to the DOF chosen in this study
- the FE grid used in this paper may not be sufficient to describe it even though it seems very appropriate for the axial rows.

Due to the low influence on total bearing life, the results produced here are deemed acceptable, though further work on the characterization of the radial row's life may be appropriate.

Based on the results in this section, the interpolation appears to work well in particular with the spline approach. The spline interpolation was thus used for the further calculations in the following sections.

5.2 Combined operating life

The lamina pressure interpolations that are explored above for 20 test cases are then performed for every single time step $i = 1, 2, ..., I$ in the aeroelastic simulations. The life of the bearing is then calculated according to Sect. 4.1 for each of these time steps, using the interpolated pressures.

Now the individual time steps are combined into a total operating life of the turbine. This process takes into account the multipliers x_i according to the Weibull distribution of the wind turbine class for DLC 1.2, and according to other, manufacturer-specific factors for the other DLCs. It also takes into account the movement that is performed in each time step, measured in degrees.

The proportion of operating movement ϕ_i is determined via

$$\phi_i = \frac{s_i}{s_1 + s_2 + \ldots + s_I} \tag{18}$$

where $s_i = x_i \mid \theta_{i+1} - \theta_i \mid$, with θ_i being the pitch angle at time step i. The sum $s_1 + s_2 + \ldots + s_I$ then gives the amount of movement a pitch bearing performs during the desired life of the turbine, typically 20 to 30 years.

The variables ϕ_i are then used to weigh the lives L_i of each time step i to obtain the final combined life L_{10}

$$L_{10} = \frac{1}{\frac{\phi_1}{L_1} + \frac{\phi_2}{L_2} + \ldots + \frac{\phi_I}{L_I}} \tag{19}$$

Eq. 19 gives the life in millions of revolutions. This can be converted to life in years by multiplying

$$L_{10,\mathrm{y}} = \frac{1}{n_{\mathrm{rev/y}}} L_{10} \tag{20}$$

with $n_{\mathrm{rev/y}}$ giving the rotations performed per year, obtained by $n_{\mathrm{rev/y}} = \sum_i^I s_i / (360° \cdot T_{\mathrm{field}})$, where T_{field} is the planned turbine life, typically 20 to 30 years.

Further factors may be multiplied with ~~the life~~ this basic fatigue life yielding a modified fatigue life. These values may be based on experience of the manufacturer, as well as on properties of the bearing like its hardening depth, raceway hardness, or desired reliabilities other than 90 % used for L_{10}, see Stammler et al. (2024). The highest factor is a suggested value of 3, see Stammler et al. (2024).

5.3 Simplified life calculation

For double-row four-point bearings, the authors proposed in Menck et al. (2020) an adjustment of the simplified life calculation in the original NREL DG03 version of Harris et al.. This adjustment occurred by changing the variable k_{M} in the following equation

$$P_{\mathrm{a}} = 0.75 \cdot F_{\mathrm{r}} + F_{\mathrm{a}} + \frac{k_{\mathrm{M}} M}{D_{\mathrm{pw}}} \tag{21}$$

where k_{M} is modified based on the FE results of the particular bearing in question. The life is then calculated as $L_{10} = (C_{\mathrm{a}}/P_{\mathrm{a}})^3$ for ball bearings. The radial load is thus included in the dynamic axial load.

In the newer version of NREL DG03 (Stammler et al., 2024), the authors attempt to modify this equation for three-row roller bearings. They suggest to calculate the life of the radial row and that of the axial rows separately. For the radial rows, they propose to use $L_{10,\mathrm{r}} = (C_{\mathrm{r}}/P_{\mathrm{r}})^{10/3}$, where $P_{\mathrm{r}} = F_{\mathrm{r}}$, and for the axial rows, they propose $L_{10,\mathrm{a}} = (C_{\mathrm{a}}/P_{\mathrm{a}})^{10/3}$ with $P_{\mathrm{a}} = F_{\mathrm{a}} + \frac{k_{\mathrm{M}} M}{D_{\mathrm{pw}}}$.

The results of this paper suggest that this is not necessary. The radial load F_{r} is very small compared to the load rating C_{r} of the radial row. Following the above described procedure, the life of the radial row is over 200 times as large as that of the axial row. This is incorrect: ~~the~~ for the current example, the actual life of the radial row is only about 10-15 times as high as that of the axial rows, see Fig. 18. The bending moment and the resulting structural deformation of the bearing therefore appears to play a larger role in the loading of the radial row than the radial load F_{r} itself.

We therefore deviate from our recommendations in Stammler et al. (2024) and propose to keep a simple formula akin to Eq. 21 for three-row roller bearings due to the following reasons:

- The procedure described in Stammler et al. (2024) significantly overestimates the life of the radial row;
- Nonetheless, the influence of the radial row on total bearing life is much smaller than that of the axial rows;
- Even if the influence of the radial row were bigger, this would not be picked up by the procedure given in Stammler et al. (2024), because it would be due to structural deformation, not due to the radial load F_r;
- The procedure described in Stammler et al. (2024) is unnecessarily complicated for a simplified approach and yields no benefits to Eq. 21 due to the abovementioned reasons.

~~Thus, the~~ Thus, for an even more simplified approach than the NREL DG03, the life of the bearing $L_{10} = (C_\mathrm{a}/P_\mathrm{a})^{10/3}$ can be determined ~~using a simplified approach as given in~~ from using just Eq. ~~21~~ 4 for C_a and Eq. 21 for P_a, if the factor k_M is adjusted. This ~~simplification could be used for further quick iteration on loads or to estimate effects of a different controller~~simplified approach can be useful for parametric studies, for example of the effect of different pitch bearings, wind speed distributions, or controllers.

It is possible for k_M for a roller bearing to be bigger than for the double-row four-point bearing in Menck et al. (2020). One has to consider that a roller bearing has a considerably higher dynamic capacity C_a than a double-row four-point (ball) bearing of comparable size. Due to this, the net effect of using a roller bearing may still yield an increase in life compared to the use of a double-row four-point bearing, even if k_M is bigger.

6 ~~Equivalent time for an accelerated fatigue life test on a pitch bearing test rig~~

~~For the test duration on a test rig, the fatigue damage of the bearing in the field can be put in relation to the fatigue damage of the bearing on the test rig. Both of these values are calculated by setting the time on the test rig T_test and in the field T_field in relation to the life on the test rig $L_{10,\mathrm{test}}$ and the field $L_{10,\mathrm{field}}$, respectively. Thus, the following must hold at the very least for a test to be representative for field behavior~~

$$\frac{T_\mathrm{test}}{L_{10,\mathrm{test}}} \geq \frac{T_\mathrm{field}}{L_{10,\mathrm{field}}}$$

~~The required minimum time on a test rig can then be calculated via~~

$$T_\mathrm{test} \geq T_\mathrm{field} \cdot \frac{L_{10,\mathrm{test}}}{L_{10,\mathrm{field}}}$$

~~This formula does not take statistical uncertainty into account. Depending on the number of bearings tested, it is recommended to consider statistical uncertainty into the equation, thereby increasing the test time.~~

~~Note that because the lives L_{10} are divided by each other, any corrective factors that may be applied to the life obtained in Eq. 20 cancel out. Therefore, it does not matter whether the L_{10} life obtained in Eq. 20 is an accurate measure of the actual L_{10} life of the bearing for the testing discussed here; so long as the formulae in this paper are proportional to the actual life, and the L_{10} lives for test and field have been determined in the same manner, the test represents the life on the turbine (with the statistical uncertainty of testing fewer bearings in mind).~~

6 Conclusions

The paper presented an approach to calculate the fatigue life of a three-row roller bearing that is used as a pitch bearing in a wind turbine. An FE model was presented and validated against experimental data from a real-scale pitch bearing test rig. The used FE modelling approach with 21 nonlinear spring elements per roller is a proper method for the simulation of realistic roller bearing deformation behaviour. Furthermore, this high number of spring elements allows an advanced implementation of the roller crowning and in turn leads to very similar pressure distributions compared to the Reusner model.

In order to narrow down the millions of aeroelastic time steps to a few FE simulations that can be calculated in reasonable time, a grid of FE simulations was determined for which the degrees of freedom of the bearing were reduced as much as possible. The three degrees of freedom that were retained are the resulting bending moment M, its load angle β, and the axial force F_z. For the axial force F_z, two extreme ends were simulated only for each grid case because analyses showed that the bearing behaved very linearly in between two extremes. The radial loads F_x and F_y where shown to correlate very closely with the bending moment components M_y and M_x and were therefore approximated with a linear fit. Blade 2 and 3 loads were averaged for each discrete load of blade 1.

This resulted in a grid of 72 FE simulations which envelop almost all load combinations of the entire aeroelastic data. For these 72 simulations, the contact pressures of all rollers were determined using a non-Hertzian contact algorithm based on Reusner (1977). Unlike the Hertzian rolling elements used in FE, the non-Hertzian algorithm allows for detection of edge stresses and is more accurate in general. A convergence analysis was carried out to determine the required amount of laminae for the non-Hertzian algorithm, which was determined to be 30 laminae, with an allowed error of 3 % compared to a reference simulation with 150 laminae. Since there were no severe cases of high edge stresses present in the bearing for all load cases that have been simulated, the life calculated with the non-Hertzian post-processing was simular to that calculated with Hertzian pressures from the FE results.

Instead of interpolating (or approximating via a regression) the forces in between the grid points, pressures were interpolated (or approximated via a regression) instead, because the non-Hertzian algorithm would take too much time to compute each single time step. The interpolation approach was validated using 20 randomly sampled test cases around nominal turbine wind speed. A cubic spline interpolation approach proved to be the best method to determine pressures in between the grid points, resulting in very low errors of 4.9 % and 2.9 % for the axial rows, and 193.6 % for the radial row, and a corresponding error of 13.7 % for the whole bearing life. The radial row life was very difficult to determine with all approaches, leading to the supposition that the grid may not be apt for the radial row because radial row pressures may mostly be affected by structural deformation. The radial row life therefore represents by far the biggest uncertainty in the final life, which was nonetheless accepted for this calculation because its life is comparatively high even considering the uncertainty. Axial rows, which are at much higher risk of failure according to the calculation, were calculated with low uncertainty.

The present paper further discussed how to calculate the life of the bearing including all operating conditions. No final life was given due to confidentiality constraints. An approximation for the equivalent load of the adapted three-row roller bearing used in this paper was proposed. While the resulting equivalent load may be substantially higher than in a double-row four-

point bearing from a previous publication, this result must be interpreted considering the fact that roller bearings have a higher dynamic capacity to begin with for comparable dimensions, therefore resulting in a higher life nonetheless. ~~Finally, the paper discussed how to calculate the required test time of a~~

While the method described in this paper was carried out on one particular turbine, the authors assume that it would also be applicable for other wind turbines using three-row roller ~~bearing on a pitch bearing test rig in order to determine whether it is appropriate for use in a given wind turbine~~bearings as pitch bearings. Slight variations, e.g. in the amount of laminae or k_{M}, may be necessary in this case.

Appendix A: Grid of FE simulations

The grid of FE simulations is given in Tables A1 and A2. Bending moments are given depending on the maximum bending moment $M_{\max}$ that was simulated in this paper. Only the sign (positive or negative) is given for F_z. Note that the upper and lower end of F_z ($+F_z$ and $-F_z$, respectively) are different in absolute magnitude, i.e., the simulations were not symmetrical around 0.

Appendix B: Test simulations

The test simulations carried out are given here in a simplified manner. Actual test simulations were simulated including all 15 DOF. This includes 5 DOF of each rotor blade bearing of the turbine. These 15 DOF are summarized into 3 here for simpler presentation, given in Table B1.

Table A1. Grid of FE simulations, part 1.

Simulation Nr.	Load angle β	Moment M	Axial load F_z
1	0°	20 % of $M_{\max}$	$-F_z$
2	0°	20 % of $M_{\max}$	$+F_z$
3	0°	40 % of $M_{\max}$	$-F_z$
4	0°	40 % of $M_{\max}$	$+F_z$
5	0°	60 % of $M_{\max}$	$-F_z$
6	0°	60 % of $M_{\max}$	$+F_z$
7	0°	80 % of $M_{\max}$	$-F_z$
8	0°	80 % of $M_{\max}$	$+F_z$
9	0°	100 % of $M_{\max}$	$-F_z$
10	0°	100 % of $M_{\max}$	$+F_z$
11	30°	20 % of $M_{\max}$	$-F_z$
12	30°	20 % of $M_{\max}$	$+F_z$
13	30°	40 % of $M_{\max}$	$-F_z$
14	30°	40 % of $M_{\max}$	$+F_z$
15	30°	60 % of $M_{\max}$	$-F_z$
16	30°	60 % of $M_{\max}$	$+F_z$
17	30°	80 % of $M_{\max}$	$-F_z$
18	30°	80 % of $M_{\max}$	$+F_z$
19	30°	100 % of $M_{\max}$	$-F_z$
20	30°	100 % of $M_{\max}$	$+F_z$
21	60°	20 % of $M_{\max}$	$-F_z$
22	60°	20 % of $M_{\max}$	$+F_z$
23	60°	40 % of $M_{\max}$	$-F_z$
24	60°	40 % of $M_{\max}$	$+F_z$
25	60°	60 % of $M_{\max}$	$-F_z$
26	60°	60 % of $M_{\max}$	$+F_z$
27	60°	80 % of $M_{\max}$	$-F_z$
28	60°	80 % of $M_{\max}$	$+F_z$
29	60°	100 % of $M_{\max}$	$-F_z$
30	60°	100 % of $M_{\max}$	$+F_z$
31	90°	0 % of $M_{\max}$	$-F_z$
32	90°	0 % of $M_{\max}$	$+F_z$
33	90°	20 % of $M_{\max}$	$-F_z$
34	90°	20 % of $M_{\max}$	$+F_z$
35	90°	40 % of $M_{\max}$	$-F_z$
36	90°	40 % of $M_{\max}$	$+F_z$

Table A2. Grid of FE simulations, part 2.

Simulation Nr.	Load angle β	Moment M	Axial load F_z
37	90°	60 % of $M_{\max}$	$-F_z$
38	90°	60 % of $M_{\max}$	$+F_z$
39	90°	80 % of $M_{\max}$	$-F_z$
40	90°	80 % of $M_{\max}$	$+F_z$
41	90°	100 % of $M_{\max}$	$-F_z$
42	90°	100 % of $M_{\max}$	$+F_z$
43	120°	20 % of $M_{\max}$	$-F_z$
44	120°	20 % of $M_{\max}$	$+F_z$
45	120°	40 % of $M_{\max}$	$-F_z$
46	120°	40 % of $M_{\max}$	$+F_z$
47	120°	60 % of $M_{\max}$	$-F_z$
48	120°	60 % of $M_{\max}$	$+F_z$
49	120°	80 % of $M_{\max}$	$-F_z$
50	120°	80 % of $M_{\max}$	$+F_z$
51	120°	100 % of $M_{\max}$	$-F_z$
52	120°	100 % of $M_{\max}$	$+F_z$
53	150°	20 % of $M_{\max}$	$-F_z$
54	150°	20 % of $M_{\max}$	$+F_z$
55	150°	40 % of $M_{\max}$	$-F_z$
56	150°	40 % of $M_{\max}$	$+F_z$
57	150°	60 % of $M_{\max}$	$-F_z$
58	150°	60 % of $M_{\max}$	$+F_z$
59	150°	80 % of $M_{\max}$	$-F_z$
60	150°	80 % of $M_{\max}$	$+F_z$
61	150°	100 % of $M_{\max}$	$-F_z$
62	150°	100 % of $M_{\max}$	$+F_z$
63	180°	20 % of $M_{\max}$	$-F_z$
64	180°	20 % of $M_{\max}$	$+F_z$
65	180°	40 % of $M_{\max}$	$-F_z$
66	180°	40 % of $M_{\max}$	$+F_z$
67	180°	60 % of $M_{\max}$	$-F_z$
68	180°	60 % of $M_{\max}$	$+F_z$
69	180°	80 % of $M_{\max}$	$-F_z$
70	180°	80 % of $M_{\max}$	$+F_z$
71	180°	100 % of $M_{\max}$	$-F_z$
72	180°	100 % of $M_{\max}$	$+F_z$

Table B1. FE test simulations.

Simulation Nr.	Load angle β	Moment M	Axial load F_z
1	52.68°	56.61 % of M_max	53.66 % of $+F_\mathrm{z}$
2	55.49°	55.29 % of M_max	62.19 % of $+F_\mathrm{z}$
3	62.50°	43.76 % of M_max	42.94 % of $+F_\mathrm{z}$
4	64.70°	89.37 % of M_max	41.87 % of $+F_\mathrm{z}$
5	66.40°	76.45 % of M_max	62.52 % of $+F_\mathrm{z}$
6	69.09°	88.16 % of M_max	66.34 % of $+F_\mathrm{z}$
7	74.63°	58.10 % of M_max	68.52 % of $+F_\mathrm{z}$
8	75.01°	53.47 % of M_max	69.52 % of $+F_\mathrm{z}$
9	75.42°	76.98 % of M_max	39.13 % of $+F_\mathrm{z}$
10	93.64°	77.04 % of M_max	35.54 % of $+F_\mathrm{z}$
11	93.65°	61.31 % of M_max	70.74 % of $+F_\mathrm{z}$
12	100.71°	61.73 % of M_max	45.85 % of $+F_\mathrm{z}$
13	100.82°	69.80 % of M_max	66.12 % of $+F_\mathrm{z}$
14	101.19°	65.07 % of M_max	72.68 % of $+F_\mathrm{z}$
15	101.85°	50.80 % of M_max	69.06 % of $+F_\mathrm{z}$
16	104.19°	76.23 % of M_max	57.73 % of $+F_\mathrm{z}$
17	106.25°	71.77 % of M_max	51.29 % of $+F_\mathrm{z}$
18	107.37°	71.10 % of M_max	54.42 % of $+F_\mathrm{z}$
19	110.58°	62.86 % of M_max	55.65 % of $+F_\mathrm{z}$
20	110.81°	57.47 % of M_max	46.81 % of $+F_\mathrm{z}$

Author contributions. OM: Conceptualization, Methodology, Software, Validation, Investigation, Writing - Original Draft, Visualization; FS: Methodology, Software, Validation, Writing - Original Draft; MS: Writing - Review & Editing

Competing interests. The authors declare no conflicts of interest.

Acknowledgements. We gratefully acknowledge funding from the European Union's Horizon 2020 research and innovation programme under grant agreement No 791875, project name ReaLCoE. We thank GE Wind for allowing this publication and we thank Valentin Radigois for his useful feedback and support. We thank Martin Geibel for generating the plots of the FE validation.

References

Becker, D.: Pitch bearings for multi-MW wind turbine applications – advanced multi-bearing calculation process and product developments trend regarding pitch bearing and hub modularization, 2024.

Becker, D. and Jorgensen, T.: Multi-MW Blade Bearing Applications – Advanced Blade Bearing Design Process and Pitch Bearing Modul Development Trends, Wind Turbine Bearings, Bremen, 2023.

Becker, D., Esderts, A., Liewen, C., Masendorf, L., Müller, P., Mevius, L., Neidnicht, M., Rollmann, J., Volmer, G., and Wächter, M., eds.: Rechnerische Festigkeitsbewertung von zyklisch hochbeanspruchten Flügelverstelllagern in Windenergie-Anlagen auf Basis der FKM-Richtlinie: Deutscher Verband für Materialforschung und –prüfung e.V, https://doi.org/10.48447/FKM-2022-014, 2022.

Bossanyi, E. A.: Individual Blade Pitch Control for Load Reduction, Wind Energy, 6, 119–128, https://doi.org/10.1002/we.76, 2003.

Burton, T., Jenkins, N., Sharpe, D., and Bossanyi, E.: Wind energy handbook, Wiley, Chichester , West Sussex, second edition edn., ISBN 978-0-470-69975-1, 2011.

Escalero, M., Olave, M., Behnke, K., and Muñiz-Calvente, M.: iKonPro®: A software for the probabilistic prediction of rolling contact fatigue, Journal of Physics: Conference Series, 2692, 012 037, https://doi.org/10.1088/1742-6596/2692/1/012037, 2024.

Graßmann, M., Schleich, F., and Stammler, M.: Validation of a finite-element model of a wind turbine blade bearing, Finite Elements in Analysis and Design, 221, 103 957, https://doi.org/10.1016/j.finel.2023.103957, 2023.

Harris, T., Rumbarger, J. H., and Butterfield, C. P.: Wind Turbine Design Guideline DG03: Yaw and Pitch Rolling Bearing Life, https://doi.org/10.2172/969722.

Harris, T. A. and Kotzalas, M. N.: Rolling Bearing Analysis, 5th Edition, Taylor & Francis, Boca Raton, 2007.

ISO: ISO 16281:2025(en): Rolling bearings – Methods for calculating the modified reference rating life for universally loaded rolling bearings, a.

ISO: ISO/TR 1281-2:2008(E) - Rolling bearings — Explanatory notes on ISO 281 — Part 2: Modified rating life calculation, based on a systems approach to fatigue stresses, b.

ISO: ISO/TR 1281-1:2021(E): Rolling bearings - Explanatory notes on ISO 281 - Part 1: Basic dynamic load rating and basic rating life, c.

ISO: ISO 281:2007(E): Rolling bearings - Dynamic load ratings and rating life, d.

Keller, J. and Guo, Y.: Rating of a Pitch Bearing for a 1.5-Megawatt Wind Turbine, https://doi.org/10.2172/1902646, 2022.

Leupold, S., Schelenz, R., and Jacobs, G.: Method to determine the local load cycles of a blade bearing using flexible multi-body simulation, Forschung im Ingenieurwesen, 85, 211–218, https://doi.org/10.1007/s10010-021-00457-y, 2021.

Lopez, A., Zurutuza, A., Olave, M., Portugal, I., Muñiz-Calvente, M., and Fernandez-Canteli, A.: Pitch bearing lifetime prediction considering the effect of pitch control strategy, Journal of Physics: Conference Series, 1222, 012 017, https://doi.org/10.1088/1742-6596/1222/1/012017, 2019.

Lundberg, G.: Elastische Berührung zweier Halbräume, Forschung im Ingenieurwesen, 10, 201–211, https://doi.org/10.1007/BF02584950, 1939.

Lundberg, G. and Palmgren, A.: Dynamic Capacity of Rolling Bearings: Proceedings of the Royal Swedish Adademy of Engineering Sciences, 196, Generalstabens Litografiska Anstalts Förlag, Stockholm, 1947.

Menck, O.: The Finite Segment Method—A Numerical Rolling Contact Fatigue Life Model for Bearings Subjected to Stochastic Operating Conditions, Journal of Tribology, 145, https://doi.org/10.1115/1.4055916, 2023.

Menck, O. and Stammler, M.: Review of rolling contact fatigue life calculation for oscillating bearings and application-dependent recommendations for use, Wind Energy Science, 9, 777–798, https://doi.org/10.5194/wes-9-777-2024, 2024.

Menck, O., Stammler, M., and Schleich, F.: Fatigue lifetime calculation of wind turbine blade bearings considering blade-dependent load distribution, Wind Energy Science, 5, 1743–1754, https://doi.org/10.5194/wes-5-1743-2020, 2020.

Menck, O., Behnke, K., Stammler, M., Bartschat, A., Schleich, F., and Graßmann, M.: Measurements and modeling of friction torque of wind turbine blade bearings, Journal of Physics: Conference Series, 2265, 022 087, https://doi.org/10.1088/1742-6596/2265/2/022087, 2022.

Popko, W.: Aero-Elastic Simulation Time Series of IWT7.5 Reference Turbine, https://doi.org/10.24406/fordatis/113.

Potočnik, R., Göncz, P., Flašker, J., and Glodež, S.: Fatigue life of double row slewing ball bearing with irregular geometry, Procedia Engineering, 2, 1877–1886, https://doi.org/10.1016/j.proeng.2010.03.202, 2010.

Reusner, H.: Druckflächenbelastung und Oberflächenverschiebung im Wälzkontakt von Rotationskörpern, 1977.

Rezaei, A., Guo, Y., Keller, J., and Nejad, A. R.: Effects of wind field characteristics on pitch bearing reliability: a case study of 5 MW reference wind turbine at onshore and offshore sites, Forschung im Ingenieurwesen, 87, 321–338, https://doi.org/10.1007/s10010-023-00654-x, 2023.

Rezaei, A., Schleich, F., Menck, O., Grassmann, M., Bartschat, A., and Nejad, A. R.: Comparative analysis of rolling contact fatigue life in a wind turbine pitch bearing with different modeling approaches, Journal of Physics: Conference Series, 2767, 052 036, https://doi.org/10.1088/1742-6596/2767/5/052036, 2024.

Sadeghi, F., Jalalahmadi, B., Slack, T. S., Raje, N., and Arakere, N. K.: A Review of Rolling Contact Fatigue, Journal of Tribology, 131, https://doi.org/10.1115/1.3209132, 2009.

Schleich, F., Chen, Z., Graßmann, M., Balzani, C., and Stammler, M.: Superelement-based acceleration of finite-element simulations of wind turbine rotors, Journal of Physics: Conference Series, 2767, 052 029, https://doi.org/10.1088/1742-6596/2767/5/052029, 2024.

Schwack, F.: Untersuchungen zum Betriebsverhalten oszillierender Wälzlager am Beispiel von Rotorblattlagern in Windenergieanlagen, Dissertation, Leibniz University Hannover, https://doi.org/10.15488/9756, 2020.

Schwack, F., Stammler, M., Flory, H., and Poll, G.: Free Contact Angles in Pitch Bearings and their Impact on Contact and Stress Conditions, https://www.researchgate.net/profile/fabian-schwack/publication/308890408_free_contact_angles_in_pitch_bearings_and_their_impact_on_contact_and_stress_conditions, 2016a.

Schwack, F., Stammler, M., Poll, G., and Reuter, A.: Comparison of Life Calculations for Oscillating Bearings Considering Individual Pitch Control in Wind Turbines, Journal of Physics: Conference Series, 753, 112 013, https://doi.org/10.1088/1742-6596/753/11/112013, 2016b.

Stammler, M.: Endurance test strategies for pitch bearings of wind turbines, Dissertation, Leibniz University Hannover, https://doi.org/10.15488/10080, 2020.

Stammler, M.: Wear test programs for roller-type pitch bearings of wind turbines, Wind Energy Science, 8, 1821–1837, https://doi.org/10.5194/wes-8-1821-2023, 2023.

Stammler, M. and Schleich, F.: Load case selection for finite element simulations of wind turbine pitch bearings and hubs, Wind Energy Science Discussions, 2024, 1–20, 2024.

Stammler, M., Schwack, F., Bader, N., Reuter, A., and Poll, G.: Friction torque of wind-turbine pitch bearings – comparison of experimental results with available models, Wind Energy Science, 3, 97–105, https://doi.org/10.5194/wes-3-97-2018, 2018.

Stammler, M., Thomas, P., Reuter, A., Schwack, F., and Poll, G.: Effect of load reduction mechanisms on loads and blade bearing movements of wind turbines, Wind Energy, 23, 274–290, https://doi.org/10.1002/we.2428, 2020.

695 Stammler, M., Menck, O., Keller, J., and Guo, Y.: Wind Turbine Design Guideline DG03: Yaw and Pitch Bearings: NREL/TP-5000-89161, https://doi.org/10.2172/2406870, 2024.